7 Hydrogen Bond Isotope Effects Studied by NMR

Hans-Heinrich Limbach, Gleb S. Denisov, and Nikolai S. Golubev

CONTENTS

I. INTRODUCTION

For a long time, Nuclear Magnetic Resonance (NMR) spectroscopy has been used to study the kinetics of hydrogen transfer in condensed phases. As NMR is traditionally regarded as a "slow"

kinetic method, systems exhibiting relatively large barriers for the proton transfer had been studied, giving rise to kinetic H/D isotope effects.[1,2] In the last years, the dynamic range of NMR has been increased into the micro- and nanosecond time scale.[2b] However, a long time ago it was also recognized that NMR is an excellent tool for the study of low-barrier hydrogen bonds, as isotope effects on NMR parameters can be observed which give interesting insights into the type of hydrogen bonds in solution.

In past years, two developments in NMR have especially promoted the understanding of H/D isotope effects on NMR parameters and hydrogen bond geometries in liquids and solids. The first is dipolar solid-state NMR from which new insights into geometric isotope effects can be obtained directly. This method is also a link between the world of hydrogen bond geometries and NMR parameters obtained in solution or in biomolecular systems. The second development is the combination of solid-state NMR methods with low-temperature liquid-state NMR methods[3] using liquefied deuterated gases such as freons as NMR solvents. The possibility to perform liquid-state NMR measurements at low temperatures allows one to observe different hydrogen bonded environments, protonated and deuterated, in the slow NMR hydrogen bond exchange regime.

The scope of this chapter is, therefore, to present examples of how liquid- and solid-state NMR can be used as a tool in order to determine the geometries of protonated and deuterated intermolecular hydrogen bonded systems in solids and liquids. Firstly, we will describe geometric correlations that provide a basis for the classification of hydrogen bonded systems. The advantage and the limits of these correlations are discussed. Then, the correlations are applied to describe geometric hydrogen bond isotope effects of single as well as of multiple hydrogen bonded systems. In a series of acid–base complexes we will deal with the determination of solvent induced temperature effects on hydrogen bond geometries and of H/D isotopic fractionation factors. Finally, we will discuss the occurrence of H/D isotope effects on the geometries of coupled hydrogen bonds.

At this point we would like to caution the reader: this review is written with the eyes of an experimental chemist who uses the simplest concepts available to describe and interpret experimental results. A description of the approximations used and their justification is beyond the scope of this review. Finally, in this book, the chapters of Hansen and Perrin review the NMR research field of H/D isotope effects of hydrogen bonded systems in solution, with special emphasis on intramolecular hydrogen bonds. The chapter of Del Bene deals with high-level quantum-mechanical calculations of strong protonated and deuterated intermolecular hydrogen bonds.

In this chapter, we will use the notion "hydron" L = H, D as a general term for mobile hydrogen isotopes such as the proton and the deuteron.

II. THEORETICAL SECTION

A. The Crystallographic View of Hydrogen Bonded Systems

The easiest way to classify hydrogen bonded systems is the geometric information available by x-ray and neutron diffraction crystallography.[4] Therefore, we will review in this section recent results of this field, especially the phenomenon of hydrogen bond correlations.

To any hydrogen bond A–H···B one can normally associate two distances, the A···H distance $r_1 \equiv r_{AH}$ for the diatomic unit AH, and the H···B distance $r_2 \equiv r_{HB}$ for the diatomic unit HB. According to Pauling,[5] one can associate to these distances so-called valence bond orders or bond valences, which are nothing else than the "exponential distances"

$$p_1 = \exp\{-(r_1 - r_1^o)/b_1\}, \quad p_2 = \exp\{-(r_2 - r_2^o)/b_2\}, \quad \text{with } p_1 + p_2 = 1 \tag{7.1}$$

where b_1 and b_2 are parameters describing the decrease of the bond valences of the AH and the HB unit with the corresponding distances. r_1^o and r_2^o are the equilibrium distances of the fictive nonhydrogen bonded diatomic molecules AH and HB. If one assumes that the total valence for

hydrogen is unity, it follows that when one distance is varied, the other automatically adjusts, leading to an ensemble of allowed r_1 and r_2 values called the hydrogen bond correlation curve. The hydrogen bond angle does not appear in Equation 7.1. This correlation implies also a correlation between the hydrogen bond coordinates $q_1 = 1/2(r_1 - r_2)$ and $q_2 = r_1 + r_2$. For a linear hydrogen bond, q_1 represents the distance of H from the hydrogen bond center and q_2 the distance between atoms A and B. We note that correlations of the type of Equation 7.1 have been used a long time ago in the context of describing the "bond energy bond order conservation" reaction pathway of the $H_2 + H$ reaction.[6]

A typical geometric hydrogen bond correlation according to Equation 7.1 is depicted in Figure 7.1a. When H is transferred from one heavy atom to the other, q_1 increases from negative values to positive values. q_2 goes through a minimum which is located at $q_1 = 0$ for AHA and near 0 for AHB systems. This correlation means that both proton transfer and hydrogen bonding coordinates can be reduced to a single coordinate s representing the pathway along the correlation curve, with $s = 0$ at $q_1 = 0$. In Figure 7.1b are depicted the corresponding valence bond orders.

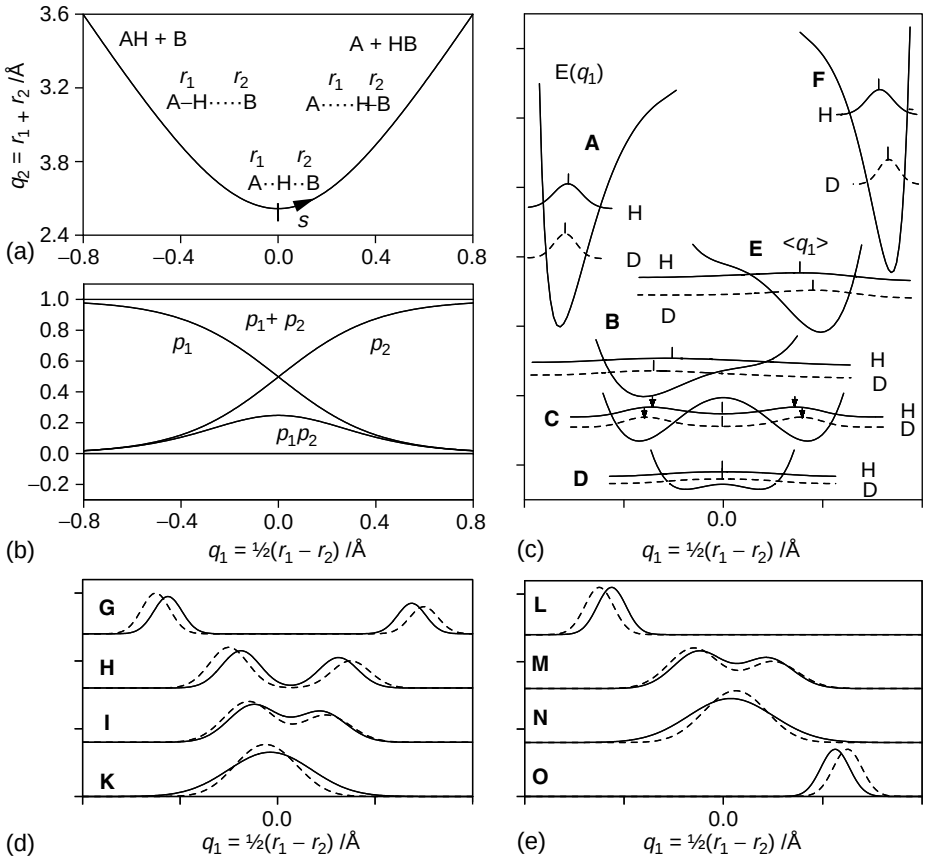

FIGURE 7.1 (a) Correlation of the hydrogen bond length $q_2 = r_1 + r_2$ with the proton-transfer coordinate $q_1 = 1/2(r_1 - r_2)$. The variable s represents the pathway along the correlation curve, with $s = 0$ at $q_1 = 0$. (b) Evolution of the valence bond orders defined in Equation 7.1. (c) One-dimensional potential energy curves (schematically) for the proton motion in hydrogen bonds. (d) Vibrationally and solvent averaged one-dimensional hydron density distribution functions of quasisymmetric hydrogen bonds of different strength. (e) Vibrationally and solvent averaged one-dimensional hydron density distribution functions of nonsymmetric hydrogen bonds of different strength. For further explanation see text.

They are unity in one and zero in the other limit. The product p_1p_2 is zero in both limits, but exhibits a maximum of 0.25 at $q_1 = 0$. The sum of both bond orders is unity.

In order to establish the parameters of Equation 7.1 used to calculate the solid line in Figure 7.1a it is necessary to know the position of the proton in the hydrogen bond. As this is a difficult task for x-ray diffraction it is not surprising that hydrogen bond correlations have been developed only recently after a large number of low-temperature neutron diffraction data have become available. Thus, parameters of Equation 7.1 have been derived empirically by Steiner et al.[7] from low-temperature neutron diffraction data for OHO, NHN, and OHN hydrogen bonds, mainly of weak and medium strength. These correlations seem also to hold for strong hydrogen bonds, as verified by dipolar solid-state NMR[8] and by theoretical calculations.[8–10]

The advantage of the correlation is that the two phenomena of hydrogen bond formation and proton transfer are linked together in a single pathway. From the crystallographic view, where proton donors and acceptors are held together not only by hydrogen bonds, there is no clear border between the free molecules and the hydrogen bonds. The usual van der Waals cutoff criterion of about 3.6 Å for A···B heavy atom distances of hydrogen bonds AHB seems to be too restrictive.[7a] Also, it is not easy to define the border line between weak, medium, and strong and short hydrogen bonds.

B. Origin of Hydrogen Bond Isotope Effects

1. Influence of the Hydron Potential

The above correlation implies that the crystallographic view of atoms in defined positions is valid. From a quantum-mechanical standpoint, atomic positions represent observables, which are averaged over the vibrational wave functions. Because of the anharmonicity of the proton potential of single- or double-well hydrogen bonded systems the averaged proton positions in hydrogen bonds do not coincide with the equilibrium positions. A general quantum-mechanical treatment of single-well hydrogen bonds has been proposed by Sokolov et al.[11]

As a detailed description of all types of hydrogen bonds is beyond the scope of this chapter, we only sketch some typical one-dimensional potentials in Figure 7.1c for a sequence of configurations where the equilibrium position of H is shifted from A to B. The squared wave functions of the lowest vibrational states are included, where the vertical bars correspond to the average hydron positions $\langle q_1 \rangle^{\mathrm{L}} \equiv q_1^{\mathrm{L}}, \mathrm{L} = \mathrm{H}, \mathrm{D}$. In principle, the one-dimensional potential curves represent averages over various zero-point motions. Therefore, they are slightly different for H and for D as indicated schematically. Note that this does not represent a deviation from the Born–Oppenheimer approximation. **A**, **B** and **E**, **F** represent configurations with asymmetric single-well potentials. **A** and **F** exhibit already a considerable Morse-type proton potential, with different average positions of H and D because of their different zero-point energy and hence different ground-state wave functions. This anharmonic effect gives rise to "geometric" H/D isotope effects on the average hydron positions. The effect is increased for the stronger hydrogen bonds **B** and **E**. We note that if other modes are taken into account, it could be that, for example, configuration pairs such as **A** and **F**, or **B** and **E**, or **A** and **E** constitute stable "tautomers" which can interconvert with each other in terms of a chemical rate process characterized by forward and backward rate constants. As the two forms of a pair are separated by a barrier, this situation is often not distinguished from a true double-well situation such as **C**, where the vibrational wave function is extended over both potential wells and exhibits two maxima indicated by arrows. The lowest vibrational levels occur in pairs, separated by a tunnel splitting, not depicted in Figure 7.1c. Such a situation is found for proton transfer in small molecular systems in the gas phase.[12] For weak and medium hydrogen bonds, solid state interactions generally lower the symmetry and lead to proton localization as shown directly by various spectroscopic techniques.[13]

Nevertheless, when the barrier is low or even negligible, situations such as **C** or **D** can exist for small values of q_1 even in condensed matter, although they may be difficult to detect. When the two maxima of the squared ground-state wave functions are well separated, two half protons can be localized by neutron diffraction, and for each position the hydrogen bond correlation may be fulfilled. In the case of **C** the proton density in the hydrogen bond center is, however, already substantial, and when the usual ellipsoid is used to fit the proton locations average H and D positions $q_1^L = 0$ may result not only for **D** but also for **C**. As both configurations exhibit different heavy atom distances, the hydrogen bond correlation will be no longer fulfilled.

2. Effects of the Environment

In polyatomic molecules, the atoms distant from the hydrogen bond provide a "bath," i.e., an intramolecular environment which influences the hydron potential for which examples were given in Figure 7.1c. There are two main phenomena that generally occur. The first concerns the nature of hydron transfer in a double-well potential. When the system is small and isolated, a double oscillator is realized with delocalized vibrational states split by hydron tunneling, for example the double proton transfer in formic acid dimer in the gas phase.[14] Increasing the size of the system and incorporation into the solid state leads to an incoherent double-proton transfer in solid benzoic acid dimer.[15] For this phenomenon also the term "tautomerism" has been used, characterized by rate constants and kinetic H/D isotope effects. If the system is asymmetric, it will also be characterized by an equilibrium constant and equilibrium isotope effects or isotopic fractionation between the tautomers. Generally, H is enriched in the tautomer exhibiting the smaller zero-point energy (see chapter of J. Bigeleisen). Not only chemical substitution lowers the symmetry, but also asymmetric isotope labeling, for example ^{17}O or ^{18}O substitution in an otherwise symmetric OHO hydrogen bond. This case will be addressed below as the "quasisymmetric" case. An equilibrium between Case **A** and **F** in Figure 7.1c would correspond to such a situation. Such systems are described in the chapter of Perrin who used the technique of isotopic perturbation in order to elucidate the symmetry of hydrogen bonds in solution.[16] A detailed description of these phenomena is beyond the scope of this chapter.

The second phenomenon is concerned with the influence of intermolecular interactions on the potential of the hydron in the hydrogen bonded system. As compared to the gas phase, the potential may be modified in the solid state. For example, a symmetric double well can become slightly asymmetric. In glassy state, a distribution of different sites is observed, where the double wells exhibit a different asymmetry.[13b] In the liquid state, the distribution of different sites will convert slowly in the IR timescale, but fast within the NMR time scale. The resulting vibrationally and solvent averaged hydron density distribution for the quasisymmetric case is depicted schematically in Figure 7.1d as a function of the hydrogen coordinate q_1 (Figure 7.1d, Case **G**). Clearly, two tautomers with different geometries are well defined. The width of the peaks is caused mainly by intermolecular interactions. As has been derived qualitatively by a discussion of IR bands, the width of the distribution can be substantial in solution, i.e., much larger than in the crystalline state.[17] As discussed above, the position of both peaks is different for H and for D, giving rise to an *intrinsic* H/D isotope effect on the hydrogen bond geometries, and hence also to modified spectroscopic parameters. D is located farther away from the hydrogen bond center as compared to H. Because of isotopic fractionation, a modified intensity distribution of the proton and the deuteron probabilities are realized as indicated schematically by the dashed line for D.

When the barrier of the hydron motion in the quasisymmetric hydrogen bonded system becomes smaller, the hydron density peaks move towards each other according to the hydrogen bond correlation of Figure 7.1a, and eventually merge. Here the case of "easily polarizable" hydrogen bonds is reached, a phenomenon studied in many papers by Zundel et al.[18] Hynes et al. (see chapter of Kiefer and Hynes) have studied the dynamics of hydron transfer under these

conditions. In this regime, the width of the hydron density distribution increases strongly. In Case **K**, the deuteron is more confined in the hydrogen bond center than the proton; however, the average H and D density can still be different as the system is only quasisymmetric. By contrast, in Case **I**, D is still farer away from the hydrogen bond center than H.

The asymmetric case is depicted in Figure 7.1e. In Case **L** only a single configuration is realized, characterized by an intrinsic geometric H/D isotope effect. When the hydron is shifted through the hydrogen bond center, similar configurations of the type **M** or **N** can be realized, which are similar to those of **I** and **K**. In these cases, it is no longer possible to distinguish *intrinsic* and *equilibrium* isotope effects: isotopic substitution does not only shift the position and the intensities of the maxima of the hydron density distribution functions but the whole functions themselves. Therefore, some of us have proposed to use the term *hydrogen bond isotope effects*[19] instead of *intrinsic* and *equilibrium* isotope effects in the case of strong hydrogen bonds.

A scenario arising from *ab initio* calculations of various acid-base complexes AHB in the presence of electric fields of Zundel et al.,[18] Del Bene et al.,[20] and Ramos et al.,[10a] which explains the distribution of hydrogen bond geometries in solution is illustrated in Figure 7.2 which is adapted from Ref. 21. The individual solvent dipoles create a temperature-dependent effective electric field at the solute site. This field is large at low temperatures where the dipoles are ordered and small at high temperatures where they are disordered. As a consequence, the temperature-dependent electric field induces in the solute a dipole moment μ that is small at high temperatures, but increases as the temperature drops. The dipole moment induced depends on the polarizability of the complex, which consists of two contributions. The electronic contribution is associated with a reorganization of the electronic cloud under the action of the electric field. The nuclear part which is also called *nuclear* or *vibrational* polarizability is associated with changes of the nuclear geometry. In a molecular complex A–H···B exhibiting a relatively small permanent electric dipole moment the latter can only be enhanced by charge transfer from B to AH. The energy for the charge separation is provided by the electric field; this energy is minimized by a contraction of the hydrogen bond. In other words, a molecular complex A–H···B contracts in the presence of an electric field. This hydrogen bond contraction is accompanied by a displacement of the proton to the hydrogen bond center. Once the proton has crossed the center, an increase of the dipole moment is achieved by a further displacement of the proton towards B, accompanied by an increase of the A···B distance.

However, the question is now whether the shortest quasisymmetric hydrogen bond configuration constitutes a transition state or the top of the barrier of a double-well potential as indicated in Figure 7.2a, or whether this state is a stationary stable state. For this purpose, it is necessary to consider the thermodynamics of these systems. Solvent reorientation around the solutes leads to a gain in energy but also requires a decrease of the entropy. Therefore, the zwitterionic forms will be more stable at low temperature as depicted in the free-energy diagrams of Figure 7.2. The conventional picture of proton transfer assumes that $A^{\delta-}\cdots H\cdots B^{\delta+}$ is a transition state as illustrated in Figure 7.2a. By contrast, Figure 7.2b represents the case of a continuous temperature-dependent distribution of stationary states exhibiting various geometries. Here, the quasisymmetric complex dominates at an intermediate "transition" temperature which is high for zwitterionic complexes and very low for molecular complexes.

Whereas in the double-well situation of Figure 7.2a H/D substitution always leads to an increase of the A···B distance, i.e., to a high-field shift of D as compared to H, the single-well situation of Figure 7.2b should lead to the opposite, i.e., a low-field shift of D as compared to H.

C. Inclusion of Quantum Corrections in Hydrogen Bond Correlations

In order to take into account zero-point stretching vibrations in the valence bond model, and hence derive a separate description of the hydrogen correlations for protonated and deuterated hydrogen

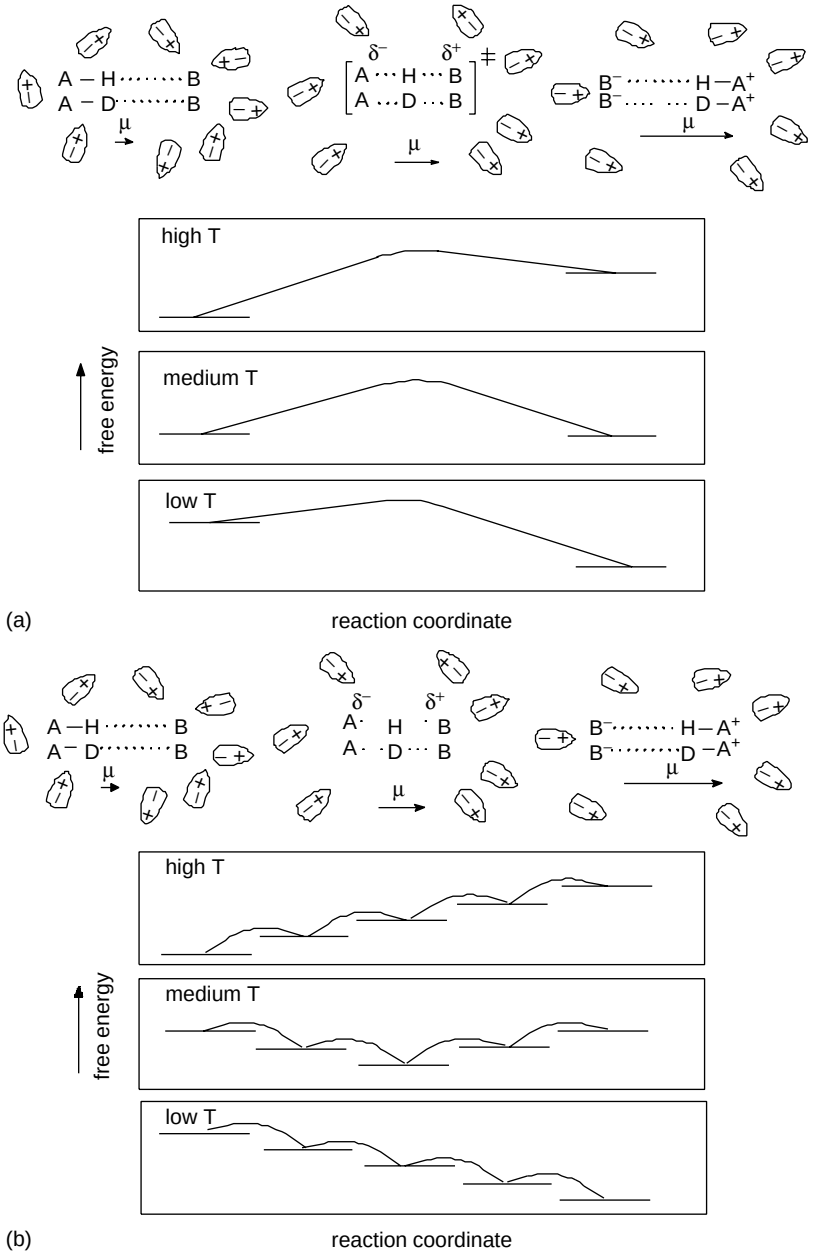

FIGURE 7.2 Temperature-dependent free-energy reaction profiles of hydron transfer in a 1:1 acid–base complex. (a) The case where $A^{\delta-}\cdots L\cdots B^{\delta+}$ corresponds to a transition state. (b) The case where $A^{\delta-}\cdots L\cdots B^{\delta+}$ corresponds to a stationary state. Both exhibit different H/D isotope effects on the hydrogen bond geometries and hence on associated NMR parameters, in particular the *primary* isotope effect $\delta(\underline{A}D\underline{B}) - \delta(\underline{A}H\underline{B})$. (*Source*: From Golubev, N. S., Shenderovich, I. G., Smirnov, S. N., Denisov, G. S., and Limbach, H. H., Nuclear scalar spin–spin coupling reveals novel properties of low-barrier hydrogen bonds in a polar environment, *Chem. Eur. J.*, 5, 492–497, 1999. With permission.)

bonds, Limbach et al.[22] have proposed that Equation 7.1 is valid only for a "classical" system exhibiting an "equilibrium" geometry corresponding to a minimum of the potential energy surface. In other words, p_1 and p_2 are essentially equilibrium bond orders. A real hydrogen bond ALB, L = H, D, experiencing anharmonic zero-point vibrations of H and D, is then characterized by the real average bond orders p_1^{L} and p_2^{L}. For the latter, Equation 7.1 may no longer be valid in the strong hydrogen bond regime, i.e.,

$$p_1^{\mathrm{L}} + p_2^{\mathrm{L}} < 1 \tag{7.2}$$

Limbach et al.[22] proposed the following empirical relations between the classical and real bond orders, which are justified by comparison with experimental data:

$$\begin{aligned} p_1^{\mathrm{L}} &= p_1 - c^{\mathrm{L}}(p_1p_2)^f(p_1 - p_2) - d^{\mathrm{L}}(p_1p_2)^g, \\ p_2^{\mathrm{L}} &= p_2 + c^{\mathrm{L}}(p_1p_2)^f(p_1 - p_2) - d^{\mathrm{L}}(p_1p_2)^g, \mathrm{L} = \mathrm{H}, \mathrm{D} \end{aligned} \tag{7.3}$$

The corresponding average distances are calculated from the real valence bond orders using Equation 7.1. The parameters c^{L} and d^{L} as well as the values of the powers f and g are empirical and have to be adjusted by comparison with experimental geometries. The term $d^{\mathrm{L}}(p_1p_2)^g$ is a correction term describing the flattening of the real correlation curves in the minimum. If $d^{\mathrm{H}} = d^{\mathrm{D}} = 0$, the classical or equilibrium correlation and the real correlation curves of AHB and ADB coincide. The "correlation" term $c^{\mathrm{L}}(p_1p_2)^f(p_1 - p_2)$ indicates then by how much the geometry of ALB is shifted on the correlation curve as compared to the classical value.

Equation 7.3 also allows one to calculate the so-called *primary geometric hydrogen bond isotope effect* (*primary* GIE)[8]:

$$\Delta q_1 \equiv q_{1\mathrm{D}} - q_{1\mathrm{H}} \tag{7.4}$$

and the *secondary geometric hydrogen bond isotope effect* (*secondary* GIE):

$$\Delta q_2 \equiv q_{2\mathrm{D}} - q_{2\mathrm{H}} \tag{7.5}$$

The *secondary* effect has also been called the *Ubbelohde effect*, as it was observed by this author and coworkers for a number of hydrogen bonded systems.[23] A negative value of Δq_2 has also been called an *inverse* Ubbelohde effect. Generally, secondary effects can be observed quite easily by x-ray crystallography, as hydron positions do not need to be determined. The primary geometric isotope effects are, however, difficult to study by x-ray diffraction, and neutron diffraction is needed. Indirect spectroscopic methods such as IR, Raman or NMR[24–26] can give more precise results after a suitable calibration of the spectroscopic parameters. Naturally, theoretical methods can also be used to calculate these geometric isotope effects.[11]

The performance of Equation 7.3 is depicted qualitatively for NHN bonds in Figure 7.3 for two arbitrary sets of parameters listed in Table 7.1. Figure 7.3a corresponds to a series of hydrogen bond configurations exhibiting a double well in the symmetric case as depicted by situation **C** in Figure 7.1c. At all geometries, Δq_2 is positive, i.e., the hydrogen bond is widened upon deuteration. Δq_1 is negative for negative values of q_1^{L} but changes sign when the latter becomes positive. In other words, D is always farther away from the hydrogen bond center than H. The bond order sum $p_1^{\mathrm{L}} + p_2^{\mathrm{L}}$ predicted by Equation 7.3 is shown on top of Figure 7.3a for the protonated and the deuterated hydrogen bonds. The deviation from unity is well pronounced in the strong hydrogen bond region; the reduction is stronger for D than for H. This reduction of the bond order sum is responsible for the larger q_2^{L} values as compared to the equilibrium geometries, where the bond order sum is always unity.

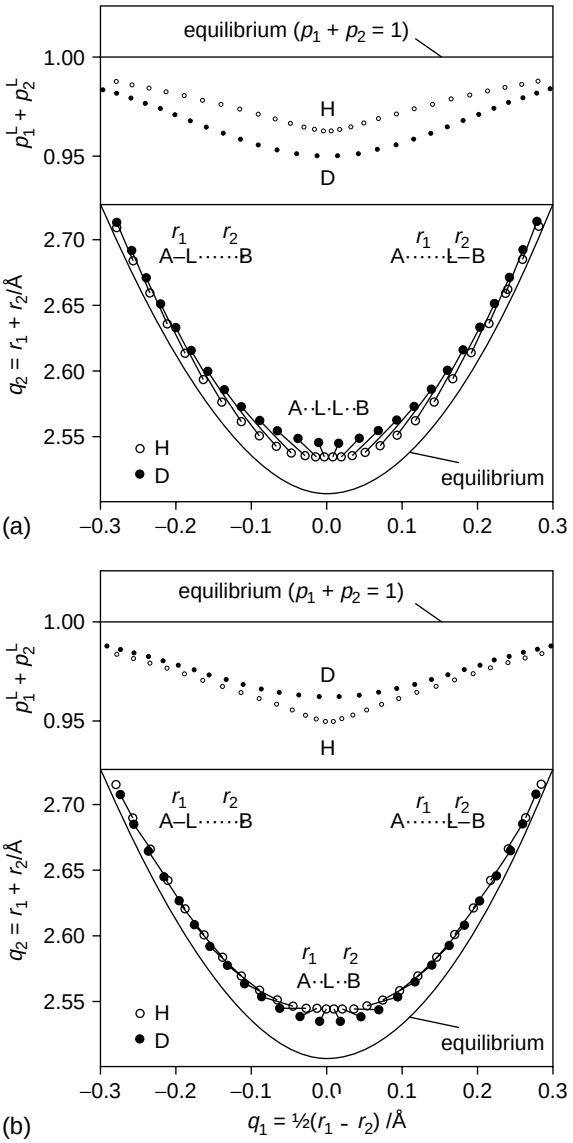

FIGURE 7.3 Geometric hydrogen bond correlations according to Equation 7.3 for systems with a strong hydrogen bond NHN, i.e., in the region around $q_1 = 0$. The solid line represents the equilibrium geometries (a) for systems with double-well proton potential at the symmetric midpoint (according to the series **A–B–C–E–F** in Figure 7.1c and b) for systems with single-well proton potential at the symmetric midpoint (according to the series **A–B–D–E–F** in Figure 7.1c). The bond order sum as a function of q_1 is shown for H and D particles both for case (a) and (b). The parameters used to calculate the curves are included in Table 7.1. For further explanation see text. (*Source*: From Limbach, H. H., Pietrzak, M., Benedict, H., Tolstoy, P. M., Golubev, N. S., and Denisov, G. S., Empirical corrections for quantum effects in geometric hydrogen bond correlation, *J. Mol. Struct.*, 706, 115–119, 2004. With permission.).

TABLE 7.1
Parameters of the Anharmonic Correction in Equation 7.3 for NHN Hydrogen Bonded Units

Figure	System	b_{NH}/Å	r^o_{NH}/Å	f	g	c^H	d^H	c^D	d^D
Figure 7.3a	NHN	0.370	0.997	5	2	330	0.3	30	0.4
Figure 7.3b	NHN	0.370	0.997	5	2	330	0.4	30	0.3
Figure 7.7	**1**, **2**, **3**	0.404	0.992	—	—	—	—	—	—
Figure 7.8	**3**	0.370	0.997	5	2	330	0.4	30	0.3
Figure 7.9	**1**, **2**	0.370	0.997	5	2	330	1.2	30	1.1

The behavior of a series of hydrogen bonded complexes exhibiting a single-well potential also in the symmetric configuration is illustrated in Figure 7.3b. In contrast to Figure 7.3a, in the symmetric case, Δq_2 is negative, i.e., the hydrogen bond is shortened upon deuteration as is well established for ions such as FHF^-.[27] Again, the sum $p_1^L + p_2^L$ for H and D is included in Figure 7.3b. Now, the hydrogen bond shortens in the symmetric case after deuteration, whereas in the asymmetric cases the contrary is found. We note that only the values of the parameters d^H and d^D needed to be exchanged in order to describe the change of the effective correlation curves between Figure 7.3a and b. For a more detailed description of the origins of deuteration effects on strong hydrogen bonds we refer to the chapter of Del Bene (Chapter 5).

D. H/D Isotope Effects on NMR Parameters and Hydrogen Bond Geometries: The Point Approximation

It is now plausible that when the geometry of a series of hydrogen bonded complexes changes in a systematic way, also the associated NMR parameters will follow. In this section, we will therefore discuss the links between the world of hydrogen bond geometries and NMR parameters. To establish such links is an important task as it opens the possibility to obtain geometric information of selected nuclei in molecules in solution where the usual diffraction or other NMR methods fail. Correlations between NMR parameters and geometries of A–H···B hydrogen bonds, for example proton chemical shifts or A···B coupling constants, have been observed using high-level *ab initio* methods by Del Bene et al. For a description of this work we refer to their chapter.

From an experimental standpoint, chemical shifts of heavy atom nuclei involved in H-bonding as well as proton chemical shifts can now be measured using high-resolution solid-state NMR techniques. The aim of such work is, therefore, to correlate experimentally the world of H-bond geometries and NMR parameters. Once such links are established, it is possible to correlate other NMR parameters measured in solution such as coupling constants across hydrogen bonds or H/D isotope effects on chemical shifts of remote atoms such as ^{13}C with the chemical shifts and hence the hydrogen bond geometries which can be used for fine tuning of H-bond geometries in solution. However, in contrast to systems with intramolecular hydrogen bonds or biomolecules where the dissociation and formation is linked to other molecular processes, the determination of intrinsic NMR parameters of intermolecular hydrogen bonds in solution is very difficult. For this task, low-temperature liquid-state NMR methods have been developed.[3]

The main task is then to establish correlations between NMR parameters and hydrogen bond geometries, i.e., the value of q_1 which would imply also a correlation with q_2. It is desirable to have isotope-insensitive correlation functions which can be applied to both the protonated and the deuterated systems. In other words, for a hydrogen bond ALB, L = H, D, the *secondary* H/D isotope effect on the chemical shifts of B

$$\Delta\delta(\mathrm{AD\underline{B}}) \equiv \delta(\mathrm{AD\underline{B}}) - \delta(\mathrm{AH\underline{B}}) \tag{7.6}$$

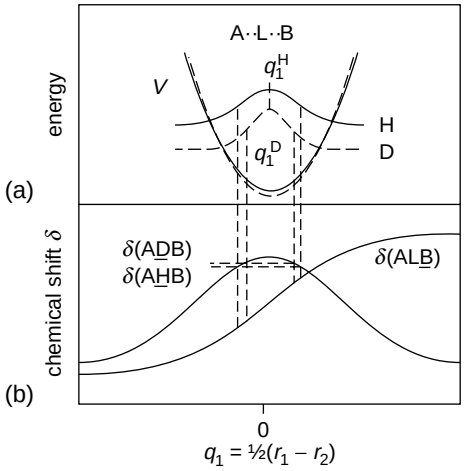

FIGURE 7.4 (a) One-dimensional potential curve and squared ground-state wave function (schematically) of a symmetric single-well hydrogen bond ALB, L = H, D. (b) Chemical shifts (schematically) of B and L as a function of q_1. The average chemical shift of D is larger than for H because of the maximum of δ(AL̲B) and the narrower wave function of D as compared to H. By contrast, as δ(ALB̲) is a linear function of q_1, δ(AHB̲) = δ(ADB̲). (*Source*: From Limbach, H. H., Pietrzak, M., Sharif, S., Tolstoy, P. M., Shenderovich, I. G., Smirnov, S. N., Golubev, N. S., Denisov, G. S., NMR- parameters and geometries of OHN- and ODN hydrogen bonds of pyridine–acid complexes. *Chem. Eur. J.*, 10, 5195–5204, 2004. With permission.)

and the *primary* isotope effects on the hydron chemical shifts

$$\Delta\delta(\text{AD̲B}) \equiv \delta(\text{AD̲B}) - \delta(\text{AH̲B}) \tag{7.7}$$

arise in this approximation only from isotope effects on the hydrogen bond geometries. Such correlations can be found for the case where the NMR parameters are in good approximation to a linear function of q_1.

This condition is normally met, except in the case of the shortest and strongest hydrogen bond in a given series of hydrogen bonds exhibiting a single-well potential as depicted in Figure 7.4. Around $q_1^H = q_1^D = 0$, the chemical shift δ(ALB̲) of a heavy atom such as ^{15}N is an almost linear function of q_1. This means that the values of δ(AHB̲) and of δ(ADB̲), averaged over the ground-state wave functions, are the same and in good approximation equal to the value at $q_1 = 0$. In other words, one can associate to each value of q_1 also a unique value δ(ALB̲). By contrast, δ(AL̲B) is a nonlinear function of q_1 exhibiting a maximum around $q_1 = 0$. As D is more confined to the hydrogen bond center as compared to H, the average value δ(AD̲B) will be larger than the average value δ(AH̲B), because the mean square values $\langle q_1^2\rangle^H$ and $\langle q_1^2\rangle^D$ are different, whereas the mean values $q_1^L = 0$ are the same for both H and D. In other words, a correlation of δ(AL̲B) with the mean average values q_1^L represents an approximation which might lead to a systematic error in the case of a symmetric single-well hydrogen bond.

It is clear that a correct description can be found only if the nuclear wave functions and the chemical shielding surface are known for the particular environment studied. An example is the FHF^- anion, where H/D isotope effects on chemical shielding have been studied theoretically by Golubev et al.[28] A theoretical analysis showed that averaging over all hydrogen bond vibrations including the bending vibrations needs to be taken into account. As such a case represents an exception at present, we will not take the breakdown of the correlation between δ(AH̲B) and q_1 for the symmetric single-well case into account in the following.

For a quantitative correlation of NMR parameters and geometries of hydrogen bonds of the type AHB, we therefore assume the validity of the following isotope-independent equations. For the chemical shifts of the base B it was assumed that[29,30]

$$\delta(\mathrm{AL\underline{B}}) = \delta(\underline{\mathrm{B}})^{\circ} p_{\mathrm{AL}}^{\mathrm{L}} + \delta(\mathrm{L\underline{B}})^{\circ} p_{\mathrm{LB}}^{\mathrm{L}} + 4\delta^{*}(\mathrm{AL\underline{B}}) p_{\mathrm{AL}}^{\mathrm{L}} p_{\mathrm{LB}}^{\mathrm{L}}, \quad \mathrm{L} = \mathrm{H}, \mathrm{D} \tag{7.8}$$

for the ^{1}H chemical shifts that

$$\delta(\mathrm{A\underline{H}B}) = \delta(\mathrm{A\underline{H}})^{\circ} p_{\mathrm{AH}}^{\mathrm{H}} + \delta(\underline{\mathrm{H}}\mathrm{B})^{\circ} p_{\mathrm{HB}}^{\mathrm{H}} + 4\delta^{*}(\mathrm{A\underline{H}B}) p_{\mathrm{AH}}^{\mathrm{H}} p_{\mathrm{HB}}^{\mathrm{H}} \tag{7.9}$$

and for scalar ^{1}H–B couplings that

$${}^{1}J(\mathrm{A\underline{HB}}) = {}^{1}J(\underline{\mathrm{HB}})^{\circ} p_{\mathrm{HB}}^{\mathrm{H}} - 8J^{*}(\mathrm{A\underline{HB}})(p_{\mathrm{AH}}^{\mathrm{H}})^{2} p_{\mathrm{HB}}^{\mathrm{H}} \tag{7.10}$$

where $\delta(\mathrm{L\underline{B}})^{\circ}$, $\delta(\underline{\mathrm{H}}\mathrm{B})^{\circ}$ and ${}^{1}J(\underline{\mathrm{HB}})^{\circ}$ represent the limiting B and ^{1}H chemical shifts and ^{1}H–B coupling constants of the fictive free HB, $\delta(\underline{\mathrm{B}})^{\circ}$ the chemical shift of the free base B, and $\delta(\mathrm{A\underline{H}})^{\circ}$ the ^{1}H chemical shift of the free acid. $\delta^{*}(\mathrm{AL\underline{B}})$, $\delta^{*}(\mathrm{A\underline{H}B})$ and $J^{*}(\mathrm{A\underline{HB}})$ are excess terms describing the deviation of the parameters of the strongest AHB hydrogen bond from the average of the limiting values of the free forms. We note that all the NMR correlation curves exhibit a principal difference to the q_1 vs. q_2 curves: the values of the latter can increase to infinity as AH moves away from B or A from HB, but the NMR parameters of the molecular units do not change any more when they are separated.

E. H/D Isotopic Fractionation, Hydrogen Bond Geometries and NMR Parameters

In contrast to the case of hydron tautomerism in strong hydrogen bonds the phenomenon of isotopic H/D fractionation is well established between different hydrogen bonded systems AHB and XHY. This equilibrium can be expressed as

$$\mathrm{AHB} + \mathrm{XDY} \rightleftarrows \mathrm{ADB} + \mathrm{XHY} \tag{7.11}$$

The equilibrium constant of this reaction is given by

$$K = 1/\Phi = \frac{x_{\mathrm{ADB}} x_{\mathrm{XHY}}}{x_{\mathrm{AHB}} x_{\mathrm{XDY}}} \approx \exp(-\Delta \mathrm{ZPE}/RT) \tag{7.12}$$

where the inverse equilibrium constant Φ is also called the fractionation factor. x_i are mole fractions or concentrations of the various isotopic species, R the gas constant, T the temperature and ΔZPE the zero-point energy difference of the hydrons in the hydrogen bonds. This quantity is given by

$$\Delta \mathrm{ZPE} = \mathrm{ZPE(XHY)} - \mathrm{ZPE(XDY)} - (\mathrm{ZPE(AHB)} - \mathrm{ZPE(ADB)}) \tag{7.13}$$

We note that Equation 7.11 does not describe H/D equilibrium isotope effects of tautomerism or, more generally, a different hydrogen or deuteron distribution within a given hydrogen bonded system, but isotopic fractionation between different systems. From a theoretical standpoint, fractionation factors are most often calculated in harmonic approximation, although anharmonic corrections are possible (see the chapters of Bigeleisen and of Wolfsberg). For hydrogen bonded systems, anharmonicities are, however, very important. Here, we conceive ΔZPE as an experimental quantity that includes all anharmonicities.

Kreevoy and Liang[31a] have determined fractionation factors of the kind in Equation 7.11 for a series of hydrogen bonded anions exhibiting a different basicities. Harris et al.[32] (see the chapter of Mildvan and references cited therein) have measured H/D isotopic fractionation factors of OHO and NHO hydrogen bonds in biomolecules in relation to the ^{1}H chemical shifts of the hydrogen

bond protons and the O···O and N···O distances. Smirnov et al.[29] have measured fractionation factors of OHN hydrogen bonded complexes.

In principle, it would be desirable to express the values of ZPE(ALB), L = H, D as a function of the corrected bond valences p_1^L and p_2^L from which ΔZPE could be calculated as a function of the hydrogen bond geometries. Unfortunately, general correlations for all isotopic sensitive vibrations and, therefore, of their ZPE values are not available at present. Therefore, we use the following approximation in which ΔZPE is expressed as a function of the classical bond valences p_1 and p_2 as has been proposed previously[29]:

$$\Delta ZPE = \Delta ZPE^{o}(4p_{OH}p_{HN})^2 + \Delta ZPE(OH)^{o}p_{OH} + \Delta ZPE(HN)^{o}p_{HN} \tag{7.14}$$

where $\Delta ZPE(OH)^{o}$ and $\Delta ZPE(HN)^{o}$ represent the zero-point energy differences of the hypothetical free diatomic states OH and HN as compared to a reference complex XHY. ΔZPE° represents the absolute drop of zero-point energy between the nonhydrogen bonded limiting states and the strongest hydrogen bonded quasisymmetric state. Equation 7.14 provides a link between the world of geometries, NMR parameters, and vibrations of hydrogen bonds.

III. APPLICATIONS

A. H/D Isotope Effects in Strong NHN Hydrogen Bonds

In this section we discuss the case of a strong NHN hydrogen bond in polycrystalline **1** and **2** (Figure 7.5), studied experimentally in Ref. 8. In Figure 7.5a are depicted the high-resolution solid-state ^{15}N NMR spectra of both compounds, before and after deuteration, obtained with $^{1}H-^{15}N$

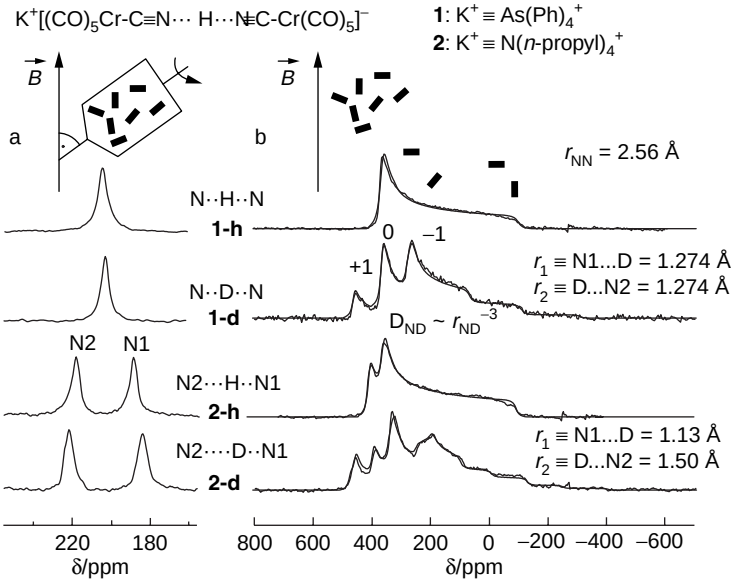

FIGURE 7.5 (a) 9.12 MHz ^{15}N {^{1}H} CPMAS NMR spectra of compounds **1-h** to **2-d** at room temperature, 2 kHz spinning speed, 9 μs 90° pulses. No temperature dependence was observed. (b) Superposed experimental and calculated 9.12 MHz ^{15}N {^{1}H} CP NMR spectra of static solid powder samples of **1-h**, **1-d**, **2-h**, **2-d** at 190 K. For the simulation of spectrum (b) a H/D fraction of 35/65 had to be taken into account. (*Source*: From Benedict, H., Limbach, H. H., Wehlan, M., Fehlhammer, W. P., Golubev, N. S., and Janoschek, R., Solid state ^{15}N NMR and theoretical studies of *primary* and *secondary* geometric H/D isotope effects on low-barrier NHN-hydrogen bonds, *J. Am. Chem. Soc.*, 120, 2939–2950, 1998. With permission.)

cross-polarization (CP) for intensity enhancement, and magic angle spinning (MAS) and ^{1}H decoupling for resolution enhancement. For **1-h** a single line is observed, indicating that both nitrogen atoms are equivalent. The line is shifted slightly to high field in **1-d**. This situation is typical for a symmetrical potential somewhere between **C** and **D** in Figure 7.1c. By contrast, for **2** two signals are obtained, indicating the presence of different nitrogen atoms N1 and N2, exhibiting different nitrogen–hydrogen distances. Here, the symmetry of the hydrogen bond is lowered by the crystal field. The chemical shift difference is much larger for **2-d** as compared to **2-h**. This finding represents the first H/D isotope effect on chemical shifts in solid-state NMR spectra. The isotope effect is explained with a distance decrease of the shorter bond and a distance increase of the longer bond after deuteration, corresponding to a proton potential of **C** in Figure 7.1c.

When the static powdered crystals are measured, the spectra of Figure 7.5b are obtained. In the case of **1-h** a typical spectrum of an axially symmetric chemical shielding tensor is obtained. Here, crystallites where the molecular N···N axis is parallel to the magnetic field B absorb at high and those perpendicular at low field. As there are more of the latter, the low-field intensity is stronger than the high-field intensity. After deuteration, a triplet splitting because of dipolar coupling of ^{15}N with ^{2}H arises. From the coupling constant D_{ND} the average inverse cubic distance r_{ND} can be obtained. The spectra of **2-d** are more complex, giving rise to two nitrogen–deuteron distances. We note that in the case of **1** the distances $r_1 \equiv N1\cdots D = r_2 \equiv D\cdots N2$ correspond to half the NN distance obtained by x-ray crystallography. From these data, a ^{15}N-chemical shift – distance correlation could be obtained, which could be used to calculate the corresponding N···H distances by extrapolation from the ^{15}N chemical shifts of **1-h** and **2-h**.

For comparison, the linear simplified system $[C{\equiv}N\cdots L\cdots N{\equiv}C]^{-}Li^{+}$(**3**) was modeled theoretically,[8] where the effects of the crystal field acting on the anion were generated by a variety of fixed C···Li distances. In principle, a more-dimensional calculation as described in the chapter of Del Bene would be desirable. In Ref. 8, for calculating the dynamical corrections of geometries of **3** a procedure based on the crude adiabatic approximation was employed. The application of this approximation consisted in an iterative procedure for the calculation of the dynamically corrected interatomic distances. For this purpose, the potential energy function $V(q_1)$ for the collinear hydron motion was calculated pointwise at fixed optimized heavy atom positions. These calculations were performed at the MP2/6 − 31 + $G(d,p)$ level. Then, the one-dimensional Schrödinger equation for the anharmonic collinear hydron motion was solved separately for L = H and D using known methods.[33] For simplicity the masses of the heavy atoms were set to infinity. The expectation value $q_1^{L} = \langle \Psi_o^{L} | q_1 | \Psi_o^{L} \rangle$, where $\Psi_o^{L}(q_1)$ represents the anharmonic vibrational ground state wave function of the hydron L = H, D, was used for calculating the distance $r_1 \equiv N1\cdots L$. Finally, the heavy atom coordinates were reoptimized keeping the distance C···Li and the dynamically corrected N1···L distance constant. This procedure was repeated until self consistency was achieved. In this way the dynamically corrected vibrational wave functions of the proton and the deuteron and the corresponding energies were obtained. Using this information the zero-point energy differences ΔZPE between the protonated and the deuterated hydrogen bond (neglecting bending contributions) and the mean linear and cubic average distances N1···L and N2···L, L = H, D, were calculated for the vibrational ground state. The results are depicted in Figure 7.6. Because of the approximation used, the average one-dimensional potential is different for the proton and the deuteron motion.

When Li^{+} is moved from the right side of the molecule to infinity, the hydron L moves from the left nitrogen to the H-bond center. At the same time, the N···N distance is reduced. The mirror process completing the L transfer is induced when Li^{+} is reapproaches from the left side. The effects on the ground-state wave function, the different H and D positions, and the zero-point energy changes are similar to those discussed in the previous section.

The analysis of **1** to **3** in terms of Equation 7.1 is shown in Figure 7.7, where neutron diffraction data of strong NHN hydrogen bonds listed in the Cambridge Structural Database (CSD)[34] are included as triangles. Figure 7.7 is taken from Ref. 22 and represents an improved version of

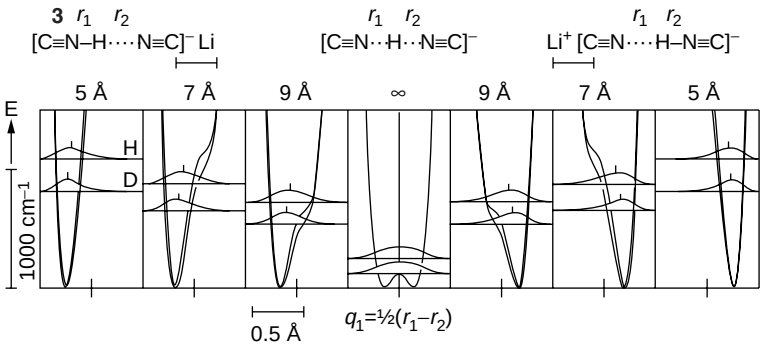

FIGURE 7.6 Calculated potential curves, vibrational ground-state energies and squares of wave functions for the proton and deuteron motion in **3-h** and **3-d**, respectively. The mean hydron positions $\langle q_1^{\mathrm{L}}(\mathrm{L})\rangle$ are indicated by vertical lines. (*Source*: From Benedict, H., Limbach, H. H., Wehlan, M., Fehlhammer, W. P., Golubev, N. S., and Janoschek, R., Solid state ^{15}N NMR and theoretical studies of *primary* and *secondary* geometric H/D isotope effects on low-barrier NHN-hydrogen bonds, *J. Am. Chem. Soc.*, 120, 2939–2950, 1998. With permission.)

corresponding graph in Ref. 8. The calculated points for **3** are fairly well located on the correlation line, calculated with the parameters $b_{\mathrm{NH}} = b_1 = b_2 = 0.404$ Å and $r^{\mathrm{o}}_{\mathrm{NH}} = r^{\mathrm{o}}_1 = r^{\mathrm{o}}_2 = 0.992$ Å proposed in Ref. 8. By contrast, the data points for **1** and **2** are systematically displaced. These deviations were not discussed in detail in Ref. 8.

The correction parameters of Equation 7.1 are obtained according to Ref. 22 by comparison of the geometries of the homoconjugated anionic systems **1** to **3**. In Figure 7.7 and Figure 7.8

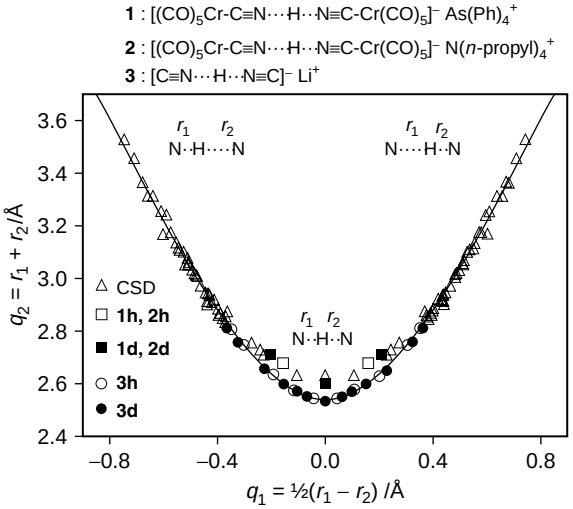

FIGURE 7.7 Correlation of the length $q_2 = r_1 + r_2$ of NHN hydrogen bonds with the proton transfer coordinate $q_1 = 1/2(r_1 - r_2)$. CSD: neutron diffraction data of various NHN hydrogen bonds from the Cambridge Structural Database.[34] The solid line was calculated in terms of Equation 7.1 with a single set of parameters $b = 0.404$ Å and $r^{\mathrm{o}} = 0.992$ Å. (*Source*: From Limbach, H. H., Pietrzak, M., Benedict, H., Tolstoy, P. M., Golubev, N. S., and Denisov, G. S., Empirical corrections for quantum effects in geometric hydrogen bond correlations, *J. Mol. Struct.*, 706, 115–119, 2004. With permission.)

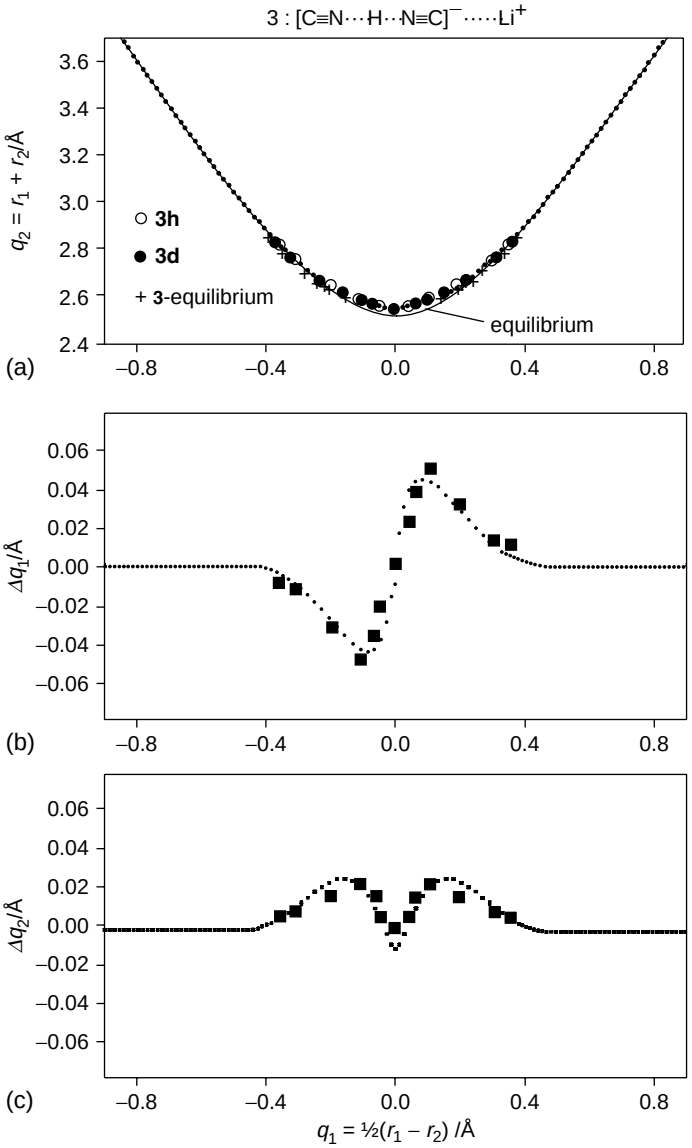

FIGURE 7.8 (a) Hydrogen bond correlations adapted to **3h** and **3d** using the correction of Equation 7.3 and the parameters listed in Table 7.1. The solid line was fitted to the equilibrium geometries of **3** listed in Table 7.2 of Ref. 8, included as crosses in the graph. (b) Primary geometric isotope effects Δq_1, (c) secondary geometric isotope effects Δq_2. (*Source*: From Limbach, H. H., Pietrzak, M., Benedict, H., Tolstoy, P. M., Golubev, N. S., and Denisov, G. S., Empirical corrections for quantum effects in geometric hydrogen bond correlations, *J. Mol. Struct.*, 706, 115–119, 2004. With permission.)

the geometric hydrogen bond correlations q_2 and the primary and the secondary geometric isotope effects Δq_1 and Δq_2 are plotted as a function of q_1. The dotted lines were calculated using Equation 7.3, where the parameters used are included in Table 7.1. The data points of Figure 7.5 are included separately in Figure 7.8a and Figure 7.9a; in addition, in Figure 7.8a are included the equilibrium distances of **3** as crosses, as calculated in Ref. 8 without dynamic correction.

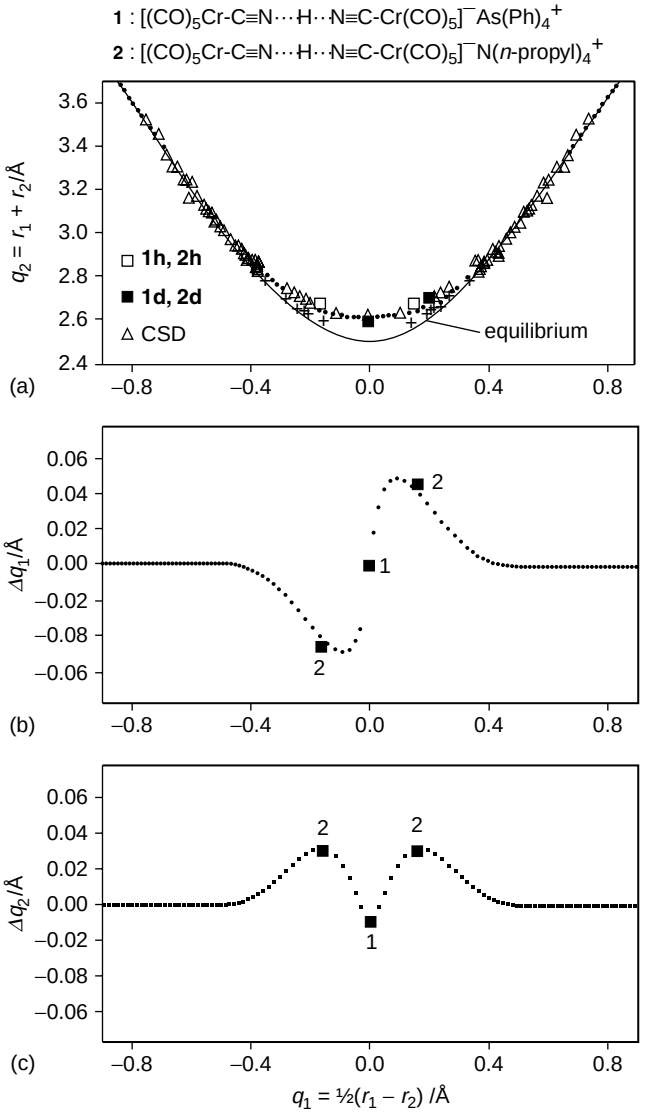

FIGURE 7.9 (a) Hydrogen bond correlations adapted to the data of **1**, **2** published in Ref. 8 and to the CSD data of Figure 7.1, using the correction of Equation 7.3 and the parameters listed in Table 7.1. (b) Primary geometric isotope effects Δq_1, (c) secondary geometric isotope effects Δq_2. (*Source*: From Limbach, H. H., Pietrzak, M., Benedict, H., Tolstoy, P. M., Golubev, N. S., and Denisov, G. S., Empirical corrections for quantum effects in geometric hydrogen bond correlations, *J. Mol. Struct.*, 706, 115–119, 2004. With permission.)

As the parameters $b_{NH} = 0.404$ Å and $r^o_{NH} = 0.992$ Å of the NHN correlation curve were derived mainly for protonated systems, they could not be directly used for the calculation of the equilibrium geometry correlation. Therefore, in Figure 7.8a, the equilibrium geometries of **3** were used for this purpose. The parameters $b_{NH} = 0.370$ Å and $r^o_{NH} = 0.997$ Å reproduced these geometries in a satisfactory way, as indicated by the crosses and the solid line in Figure 7.8a. However, one can anticipate that these parameters might be subject to changes in the future.

The computational data of the model compound **3h** and **3d** need a relatively small correction for the anharmonic zero-point vibration, as indicated by the dotted line in Figure 7.9a; the primary GIE and the secondary GIE are well reproduced. A negative secondary isotope effect is predicted at $q_1 = 0$. However, the crude adiabatic approximation used for data points of system **3** does not predict any GIE at $q_1 = 0$, because, in contrast to the expectations of Figure 7.1c, it uses the same potential for H and D for the symmetric complex (Figure 7.6). A more-dimensional treatment would probably reveal a negative secondary GIE, found experimentally for **1** as depicted in Figure 7.9a and 9c. In the cases of **1** and **2,** the correction terms (Table 7.1) are larger than for **3**; Figure 7.9 illustrates that the GIE are well reproduced. However, the most important point is that the increase in the q_2^L values of both compounds as compared to the values calculated from the equilibrium correlation is now well reproduced.

B. H/D Isotope Effects in OHN Hydrogen Bonded Pyridine–Acid and Collidine–Acid Complexes

In this section, we will analyse in particular the relations between the NMR parameters and hydrogen bond geometries of 1:1 collidine (2,4,6-trimethylpyridine)–acid and pyridine–acid complexes in different environments. The former had been studied both by solid-state NMR[35a] as well as by low-temperature liquid-state NMR using a liquefied freon gas mixture CDF_3/CDF_2Cl as NMR solvents.[36] The pyridine–acid complexes in freons have been studied in several papers.[30,19]

1. Low-Temperature NMR Spectroscopy of Pyridine–Acid Complexes Dissolved in Liquefied Freon Mixtures

As an example of solid-state NMR was already been discussed above, we will give here only an example of the liquid-state work. Figure 7.10 depicts some low temperature NMR spectra of samples of *o*-toluic acid (a–c) and of 2-thiophenecarboxylic acid (d–f) as proton donors AH in the presence of a small excess of pyridine-^{15}N as base B in CDF_3/CDF_2Cl.[19a] The deuterium fractions in the mobile proton site was about 80%. Under the conditions employed, hydrogen bond exchange is slow in the NMR timescale. The signals of the H-bond protons are split into doublets by scalar coupling with ^{15}N. The coupling constant J(O$\underline{\text{H}}$N) between ^{15}N and the hydrogen bond proton is relatively small (12 Hz) in the case of *o*-toluic acid as proton donor, indicating that the proton is preferentially localized near A, but is much larger (57 Hz) in the case of 2-thiophenecarboxylic acid, indicating that the proton is located near B. This result is plausible as 2-thiophenecarboxylic acid exhibits a greater acidity or proton donating power in comparison to *o*-toluic acid. The low field shift from 18.68 to 21.33 ppm indicates also a shortening of the OHN hydrogen bond. The ^{2}H NMR spectra (Figure 7.10b and e) of the same samples reveal primary upfield isotope shifts $\Delta\delta(\text{O}\underline{\text{D}}\text{N}) \equiv \delta(\text{O}\underline{\text{D}}\text{N}) - \delta(\text{O}\underline{\text{H}}\text{N})$ which are negative in both cases. In other words, both hydrogen bonds are weakened by D-substitution. The ^{15}N spectra give interesting additional information. Firstly, hydrogen bonding and proton transfer to pyridine leads to a high field shift of the pyridine ^{15}N signal, where the chemical shift scale of Figure 7.10 refers to the absorption of free pyridine. These high field shifts are in accordance with the increase of J(O$\underline{\text{H}}$N). However, in the 80% deuterated samples two lines appear where the more intense line arises from the deuterated complexes ODN and the smaller line from OHN which are in slow exchange. We observe that the one-bond isotope effect across the hydrogen bond $\Delta\delta(\text{OD}\underline{\text{N}}) \equiv \delta(\text{OD}\underline{\text{N}}) - \delta(\text{OH}\underline{\text{N}})$, is negative in the case of *o*-toluic acid, but positive in the case of 2-thiophenecarboxylic acid. Qualitatively, these effects can be explained in terms a widening of the hydrogen bond upon deuteration, and a larger shift of D away from the hydrogen bond center as compared to H.

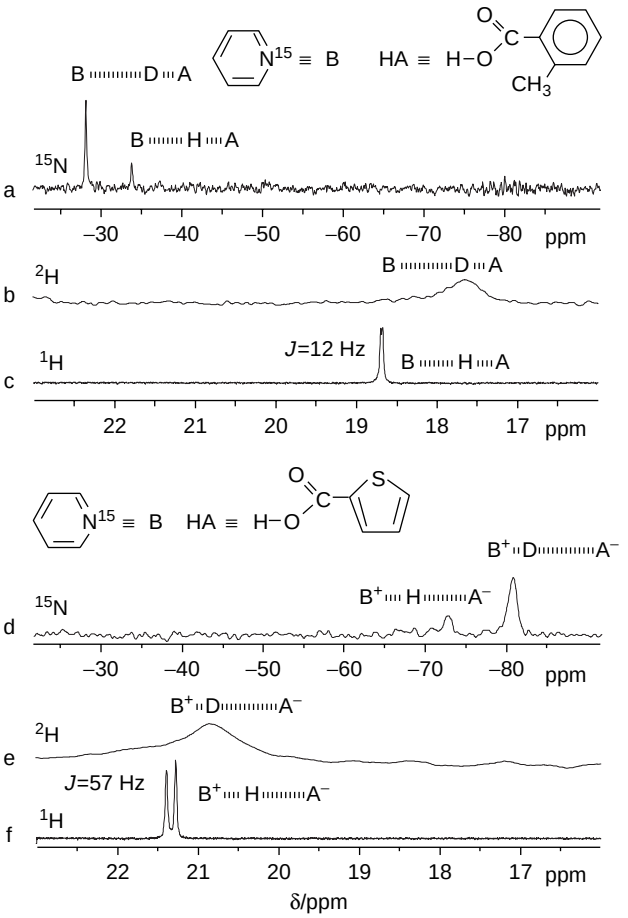

FIGURE 7.10 ^{15}N NMR (a,d), ^{2}H NMR (b,e), ^{1}H NMR (c,f) spectra (^{1}H Larmor frequency 500.13 MHz) of solutions of pyridine-^{15}N (B) and carboxylic acids (AL, L = H, D) in a 1:2 mixture of CDF_3/CDF_2Cl at a deuterium fraction in the mobile proton sites $x_D = 0.8$. a–c: 125 K, $C_B = 0.033$ M, $C_{AH} + C_{AD} = 0.028$ M, d–f: 110 K, $C_B = 0.045$ M, $C_{AH} + C_{AD} = 0.035$ M. The ^{15}N chemical shifts are referred to internal free pyridine, where $\delta(CH_3NO_2) = \delta(C_5H_5N) - 69.2$ ppm, and $\delta(NH_4Cl) = \delta(CH_3NO_2) - 353$ ppm. (*Source*: From Smirnov, S. N., Golubev, N. S., Denisov, G. S., Benedict, H., Schah-Mohammedi, P., and Limbach, H. H., Hydrogen/deuterium isotope effects on the NMR chemical shifts and geometries of intermolecular low-barrier hydrogen bonded complexes, *J. Am. Chem. Soc.*, 118, 4094–4101, 1996. With permission.)

2. Geometric Hydrogen Bond Correlations of OHN Hydrogen Bonded Complexes

In order to correlate NMR parameters with hydrogen bond geometries, Limbach et al.[37] have recently introduced the empirical corrections of Equation 7.3 into the geometric correlation analysis of OHN hydrogen bonds studied previously by Steiner.[7d] Using his parameters, which are listed in the first row of Table 7.2, the classical or equilibrium correlation was obtained as depicted by the lower solid line in Figure 7.11a. The data points of the weak and medium hydrogen bonds from the CSD from which these parameters were derived are represented by filled circles in Figure 7.11a. The filled squares stem from data obtained by Lorente et al. for 1:1 hydrogen bonded complexes of collidine with various acids using a combination of dipolar solid-state NMR[35a] and x-ray crystallography.[35b] The filled triangles in Figure 7.11a stem from the low-temperature neutron

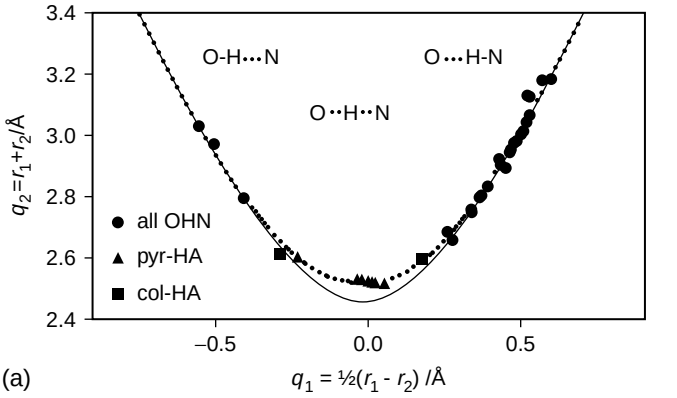
O-H···N
O···H-N
O··H··N
all OHN
pyr-HA
col-HA
$q_2 = r_1 + r_2$/Å
$q_1 = ½(r_1 - r_2)$ /Å

(a)

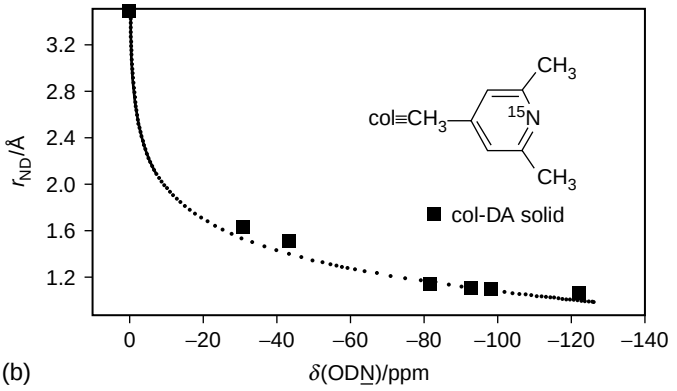
col≡CH3
15N
CH3
CH3
col-DA solid
r_{ND}/Å
δ(OD<u>N</u>)/ppm

(b)

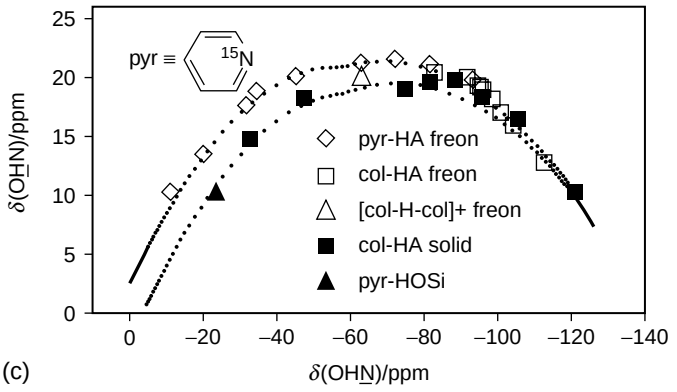
pyr ≡
15N
pyr-HA freon
col-HA freon
[col-H-col]+ freon
col-HA solid
pyr-HOSi
δ(O<u>H</u>N)/ppm
δ(OH<u>N</u>)/ppm

(c)

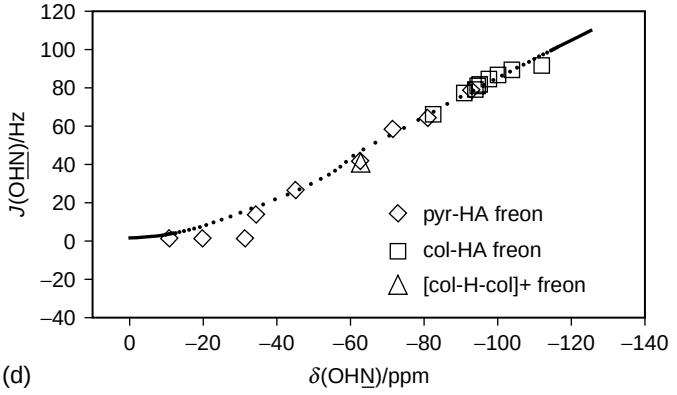
pyr-HA freon
col-HA freon
[col-H-col]+ freon
J(O<u>H</u>N)/Hz
δ(OH<u>N</u>)/ppm

(d)

TABLE 7.2
Parameters of the Geometric Hydrogen Bond Correlations of Pyridine–Acid and Collidine–Acid Complexes

Systems	b_{OH}/Å[a]	$r_{OH}°$/Å[a]	b_{HN}/Å[a]	$r_{NH}°$/Å[a]	f	g	c^H	d^H	c^D	d^D
Weak and medium strong OHN bonds	0.371	0.942	0.385	0.992	0	0	0	0	0	0
Pyridine–HA and collidine–HA in CDF_3/CDF_2Cl	0.371	0.942	0.385	0.992	5	2	360	0.7	50	0.6
Pyridine–HA and collidine–HA solid	0.371	0.942	0.385	0.992	5	2	360	0.7	110	0.6

[a] Taken from Ref. 7d. Reproduced from Ref. 37.

diffraction data of the very strong OHN hydrogen bonds between 4-methylpyridine and pentachlorophenol and related compounds.[38] As in the NHN case, systematic deviations from the equilibrium curve are observed. The dotted curve was calculated using the correction parameters listed in Table 7.2 by fitting the neutron diffraction data of the various OHN hydrogen bonds.

3. H/D Isotope Effects on the NMR Parameters of Pyridine–Acid and Collidine–Acid Complexes

A quantitative analysis of all pyridine–acid and collidine–acid data available was performed by Limbach et al.[37] and is depicted in Figure 7.11b to d and Figure 7.12. The dotted lines were calculated using the equations presented in the Theoretical section. For that purpose, A was identified with O, and B with N. In Figure 7.11b are plotted the ND distances r_{ND} of deuterated polycrystalline collidine–acid complexes as a function of their ^{15}N chemical shifts $\delta(OD\underline{N})$. The distances had been obtained previously from the dipolar ^{15}N-D couplings, and the ^{15}N chemical shifts by high-resolution solid-state NMR.[35] The parameters of equations used to calculate the dotted lines are assembled in Table 7.3.

For the case of collidine–acid complexes, the values of $\delta(OD\underline{N})$ are referenced to the ^{15}N chemical shift of neat frozen collidine, resonating at 268 ppm,[35] and those of the pyridine–acid complexes to neat frozen pyridine, resonating at 275 ppm with respect to solid $^{15}NH_4Cl$.[39] Small upfield solvent shifts $\Delta\delta(\underline{N})°$ describing the difference of the ^{15}N chemical shifts of the free bases dissolved in CDF_3/CDF_2Cl, arising from weak solute–solvent H-bond interactions were taken into account in Figure 7.11.

In Figure 7.11c are depicted the ^1H chemical shifts $\delta(O\underline{H}N)$ of the pyridine– and collidine–acid complexes obtained under various conditions as a function of the ^{15}N chemical shifts $\delta(OH\underline{N})$. The filled symbols refer to the solid collidine–acid complexes with OHN hydrogen bonds, whereas

FIGURE 7.11 OHN hydrogen bond correlations. The parameters of the calculated curves are listed in Table 7.2 and Table 7.3. (a) Geometric OHN hydrogen bond correlations. OHN: neutron diffraction data in the Cambridge Structural Database as published by Steiner[7d]; pyr–HA: neutron diffraction data of the crystalline 4-methylpyridine-pentachlorophenol complex[38]; coll–HA solid: dipolar NMR of crystalline collidine–acid complexes.[35] (b) ND distance — ^{15}N chemical shift correlation for polycrystalline collidine–acid complexes obtained by dipolar solid-state NMR.[35] (c) $^1H-^{15}N$ chemical shift correlation of pyridine–acid and collidine–acid complexes. Open symbols: CDF_3/CDF_2Cl solution at low temperatures[36,19a]; $[col-H-col]^+$ freon: Ref. 41; pyr–HOSi: pyridine in mesoporous silica.[40] (d) Correlation between the $H^{15}N$ scalar couplings $J(O\underline{H}N)$ with the ^{15}N chemical shifts of pyridine–acid and collidine–acid complexes in CDF_3/CDF_2Cl at low temperatures. (*Source*: From Limbach, H. H., Pietrzak, M., Sharif, S., Tolstoy, P. M., Shenderovich, I. G., Smirnov, S. N., Golubev, N. S., Denisov, G. S., NMR- parameters and geometries of OHN- and ODN hydrogen bonds of pyridine–acid complexes. *Chem. Eur. J.*, 10, 5195–5204, 2004. With permission.)

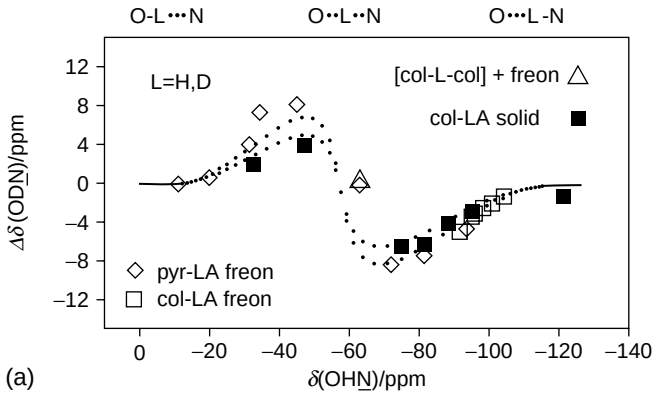
O-L•••N
O••L••N
O•••L-N
L=H,D
[col-L-col] + freon
col-LA solid
pyr-LA freon
col-LA freon
Δδ(ODN)/ppm
δ(OHN)/ppm

(a)

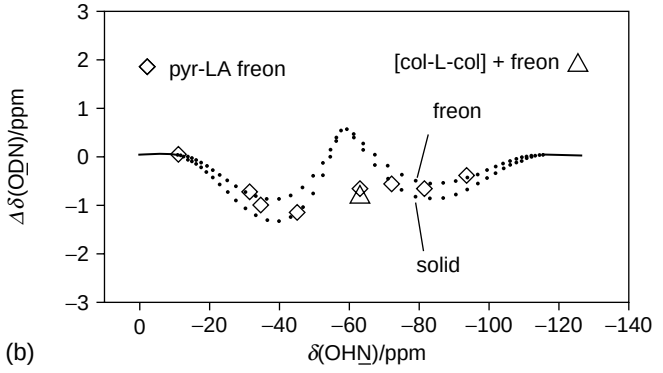
pyr-LA freon
[col-L-col] + freon
freon
solid
Δδ(ODN)/ppm
δ(OHN)/ppm

(b)

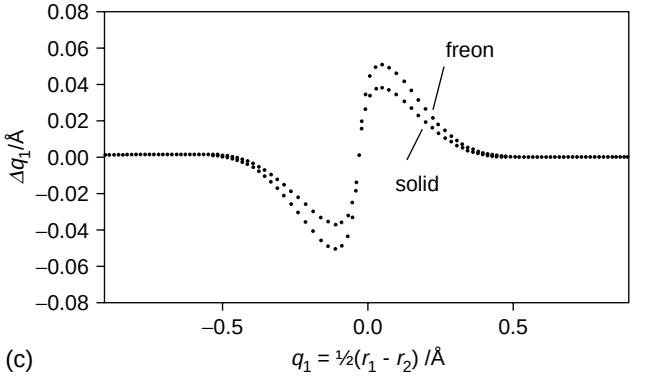
freon
solid
Δq1/Å
q1 = ½(r1 - r2) /Å

(c)

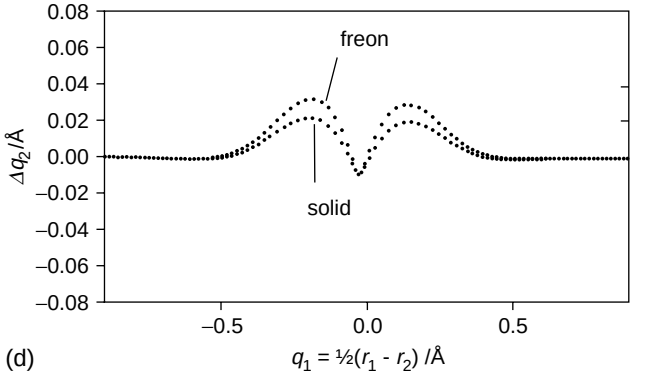
freon
solid
Δq2/Å
q1 = ½(r1 - r2) /Å

(d)

in Figure 7.11b the corresponding complexes with ODN hydrogen bonds were depicted; in addition, a data point is included as solid triangle on the left side, characterizing the complex of pyridine with surface Si–OH groups of mesoporous silica of the MCM-41 and SBA-15 type.[40] For this complex an ^{1}H chemical shift of 10 ppm and a ^{15}N chemical shift of -23 ppm with respect to frozen neat pyridine had been obtained. The open symbols refer to various pyridine–acid complexes[19a] and of collidine–acid[36] complexes dissolved in CDF_3/CDF_2Cl mixtures (freon), as well as one data point referring to the homoconjugate cation of [collidine–H–collidine]$^{+}$ reported in Ref. 41.

The data indicate that the ^{1}H chemical shifts are larger for freon solution as compared to the solid state as long as H is closer to oxygen or in the hydrogen bond center. In particular, the maximum ^{1}H chemical shift is about 21.5 ppm for freon solution, but only about 19 ppm for the solid state. We found that we were able to reproduce these findings by using the same values of $\delta(\underline{H}N)^{\circ} = 7$ ppm for "free" collidinium and pyridinium, the same excess term $\delta^{*}(O\underline{H}N) = 20$ ppm, but different values of $\delta(O\underline{H})^{\circ}$. For freon solution we had used previously a value of $+2$ ppm[29] which we kept here, and for "free" oxygen acids in the solid-state values between -2 ppm[42] and -4 ppm had been reported.[43] We found that a slightly modified value of -3 ppm fitted better the solid-state data of Figure 7.11c. The calculated dotted lines reproduce now the experimental data in a very satisfactory way.

Finally, Figure 7.11d illustrates how the scalar couplings $^{1}J(O\underline{H}N)$ between ^{1}H and ^{15}N correlate with $\delta(OH\underline{N})$. The parameters of Equation 7.10 leading to the dotted line are included in Table 7.3.

We come now to the problem of H/D isotope effects on NMR chemical shifts and geometries of the OHN hydrogen bonds studied. The secondary H/D isotope effect on the ^{15}N chemical shifts $\Delta\delta(OD\underline{N}) \equiv \delta(OD\underline{N}) - \delta(OH\underline{N})$ depicted in Figure 7.12a have been measured for pyridine–acid complexes in freon,[19a] and for collidine–acid complexes in the solid state[35a] and in freon,[36] whereas the primary isotope effects on the hydron chemical shifts $\Delta\delta(O\underline{D}N) \equiv \delta(O\underline{D}N) - \delta(O\underline{H}N)$ depicted in Figure 7.12b could be obtained only for the pyridine–acid complexes in freon.[19a] Because of the point approximation used, in order to calculate the dotted lines in Figure 7.12, it was only needed to adapt the values of the correction parameters c^{D} and d^{D} in Equation 7.3 listed in Table 7.2, as the NMR parameters in Table 7.3 were already known from Figure 7.10. Again, two data sets were obtained, one for the complexes in freon and the other for the solid state. Then, we calculated the corresponding ODN correlation curve q_2 vs. q_1. As these curves almost coincided with the dotted OHN curve of Figure 7.10a, it was not included in this graph. Instead, we calculated the isotope effects on the hydrogen bond geometries for the freon data which are included as dotted lines in Figure 7.12c and d.

The values of $\Delta\delta(OD\underline{N})$ change sign when H is moved across the hydrogen bond center; the absolute maximum and minimum values of $\Delta\delta(OD\underline{N})$ are the same. By contrast, the absolute values of $\Delta\delta(O\underline{D}N)$ in two minima are unequal. This effect arises mainly from the smaller variation of the hydron chemical shifts with the distance from the hydrogen bond center when the proton is closer to nitrogen as compared to oxygen, i.e., because of the different slopes of the ^{1}H vs. ^{15}N curves depicted in Figure 7.11c. Thus, the graphs of Figure 7.12a and b represent the NMR analogs

FIGURE 7.12 (a) Secondary $\Delta\delta(OD\underline{N}) \equiv \delta(OD\underline{N}) - \delta(OH\underline{N})$ and (b) primary $\Delta\delta(O\underline{D}N) \equiv \delta(O\underline{D}N) - \delta(O\underline{H}N)$ isotope effect on NMR chemical shifts of pyridine–acid and collidine–acid complexes around 130 K, dissolved in CDF_3/CDF_2Cl and solid collidine–acid complexes, data from Refs. 35a,36,41. (c) Primary geometric isotope effects Δq_1 and (d) secondary geometric isotope effects Δq_2 of pyridine–acid and collidine–acid complexes. The dotted curves in (a) to (d) were calculated using the parameters listed in Tables 7.2 and Table 7.3. (*Source*: From Limbach, H. H., Pietrzak, M., Sharif, S., Tolstoy, P. M., Shenderovich, I. G., Smirnov, S. N., Golubev, N. S., Denisov, G. S., NMR- parameters and geometries of OHN- and ODN hydrogen bonds of pyridine–acid complexes. *Chem. Eur. J.*, 10, 5195–5204, 2004. With permission.)

TABLE 7.3
Parameters of the NMR Hydrogen Bond Correlations of Pyridine–Acid and Collidine–Acid Complexes

Systems	$\delta(\underline{N})°$/ppm[a]	$\delta(H\underline{N})°$/ppm	$\Delta\delta(\underline{N})°$/ppm[b]	$\delta(O\underline{H})°$/ppm
Pyridine–HA in CDF_3/CDF_2Cl	0	126	−4	2
Collidine–HA in CDF_3/CDF_2Cl	0	126	−8	2
Solid collidine–HA	0	126	0	−3
	$\delta(\underline{H}N)°$/ppm	$\delta^*(O\underline{H}N)$/ppm	$^1J(\underline{H}N)°$/Hz	$J^*(O\underline{H}N)$/Hz
Pyridine–HA in CDF_3/CDF_2Cl	7	20	110	12.5
Collidine–HA in CDF_3/CDF_2Cl	7	20	110	12.5
Solid collidine–HA	7	20	—	—

[a] With respect to neat frozen pyridine and collidine, resonating at 275 ppm and 268 ppm with respect to solid NH_4Cl.[35a]
[b] $\Delta\delta(\underline{N})°$: ^{15}N chemical shift difference between the free bases in the frozen solid state and in freon solution around 130 K.

of the corresponding graphs of the geometric isotope effects depicted in Figure 7.12c and d which exhibit only slight asymmetries because of the different parameters of OH and HN bonds in Table 7.2.

The values observed for pyridine– and collidine–acid complexes in freon coincide within the margin of error. Moreover, in the zwitterionic regime, the values for the complexes in the liquid and the solid state are also very similar. By contrast, in the "molecular complex" regime where H is closer to oxygen, smaller absolute isotope effects are observed for the solids. Unfortunately, the origin of the different isotope effects in the liquid and the solid state could not be elucidated in this study.

The parameter c^D influences the curves in Figure 7.12a and c, and c^D as well as d^D influence the curves of Figure 7.12b and d. The liquid- and solid-state data are described by two different dotted curves of which the parameters are listed in Table 7.2. Besides the values of $\Delta\delta(O\underline{D}N)$ for the quasisymmetric pyridine–formic acid complex and the [collidine–H–collidine]$^+$ cation, the agreement of the calculated curves with the experimental values is satisfactory.

We note that the correction parameters c^H, d^H, c^D and d^D are very close to those found for the NHN hydrogen bonds[22] described above, where geometric data could directly be analyzed. The agreement gives confidence that the corresponding graphs in Figure 7.12c and d of the geometric H/D isotope effects on the hydrogen bond are close to the reality.

So far, we have not yet discussed the data points of the homoconjugate [collidine–H–collidine]$^+$ cation represented by open triangles in Figure 7.11 and Figure 7.12. The data point in Figure 7.11c is located below the $^{15}N-^1H$ correlation curve. As the OHN and NHN hydrogen bond geometric correlations are similar, this means that the corresponding data point in Figure 7.11a would be located around $q_1 = 0$, but the value of q_2 would be larger than the minimum value. This effect could arise either from an intrinsic barrier between two degenerate potential wells of the kind depicted in type **C** of Figure 7.1c, or from a solvent barrier, where an asymmetric structure of the type **B** depicted in Figure 7.1c exchanges rapidly with the corresponding structure exhibiting a potential corresponding to the mirror image of **B**. These interpretations are supported by the observation of a negative primary H/D isotope effect $\Delta\delta(O\underline{D}N)$ (Figure 7.12b), indicating that deuteration increases the hydrogen bond length, a sign that H is not located in the hydrogen bond center.

This finding is not in agreement with our treatment, which did not take into account two interconverting forms separated by a barrier. Thus, the correction parameters leading to the dotted

lines in Figure 7.12 predict a sign change of $\Delta\delta$(OD̲N) for the quasisymmetric complexes, as expected for systems with single well potentials in the strongest hydrogen bonds. Such a sign change had been observed for solid complexes exhibiting strong NHN hydrogen bonds,[22] as well as for systems such as FHF^-.[41] Therefore, the calculated values of $\Delta\delta$(OD̲N) in Figure 7.12b deviate from the experimental ones found for freon solution. We did not attempt here to introduce a correction for this effect, in view of the fact discussed in the Theoretical section that the point approximation breaks down anyway in the case of the values of $\Delta\delta$(OD̲N) of very strong hydrogen bonds. The agreement between the experimental and calculated values in Figure 7.12b outside the region of the symmetric hydrogen bonds is better; here double wells will not be realized because of the large asymmetries of these complexes.

In order to make further progress in this field, it will be necessary to measure the values of $\Delta\delta$(OD̲N) for the symmetric or quasisymmetric complexes not only for freon solution but also for the solid state. This task is, however, not easy in view of the large quadrupole coupling constant of D, and in view of the smaller gyromagnetic ratio of D as compared to H.

4. H/D Isotopic Fractionation and NMR Parameters of Pyridine–Acid Complexes

Some time ago, Smirnov et al.[19a] performed a low-temperature NMR study of isotopic fractionation in the series of the 1:1 hydrogen bonded acid–pyridine complexes dissolved in CDF_3/CDF_2Cl according to Figure 7.13a. In particular, using the triphenylmethanol–pyridine complex as a reference the values of K had been determined around 130 K and correlated with the hydrogen bond geometries and ^{15}N chemical shifts using Equation 7.14. Recently,[37] the data analysis was improved by taking into account the empirical correction terms of Equation 7.3. Because of the close correlation with the geometric H/D isotope effects discussed in the previous section, we will discuss this case in more detail.

In Figure 7.13b are depicted both the values of K as well as those of ΔZPE calculated according to Equation 7.12 as a function of the nitrogen chemical shift, serving again as a measure of q_1. The K values are also plotted in Figure 7.13c as a function of the ^1H NMR chemical shifts. A systematic correlation with both NMR parameters and hence the hydrogen bond geometries is observed. The dotted lines in Figure 7.13b were calculated neglecting differences of the zero-point energies in the free OH– and HN– acids using the following parameters:

$$\Delta ZPE^o = -3.13\ \text{kJmol}^{-1},\ \ \Delta ZPE(OH)^o \approx \Delta ZPE(HN)^o \approx +0.4\ \text{kJmol}^{-1} \qquad (7.15)$$

with the other parameters of Table 7.2 and Table 7.3. Thus, a zero-point energy drop of about 3.5 kJmol^{-1} between the free reference states and the strongest OHN hydrogen bond configuration is obtained. Without the correction, only a value of about 2.8 kJmol^{-1} is obtained[19a]; this value corresponds to the difference between the ZPE in the limits and the effective ZPE in the minimum of the upper curve in Figure 7.13b. If the strongest OHN configuration were a classical transition state of a single H transfer reaction, one would expect a kinetic H/D isotope effect at 298 K of $k^H/k^D \approx \exp(\Delta ZPE^o/RT) \approx 3.5$ for the new and 3.1 for the old value. Often larger values of k^H/k^D are assumed for this kind of reactions.[44] The present analysis therefore supports the idea that larger kinetic isotope effects than $k^H/k^D \approx 4$ at 298 K will arise from tunneling contributions rather than from the loss of zero-point energy in the transition state.

C. Temperature-Induced Solvent H/D Isotope Effects on NMR Chemical Shifts of FHN Hydrogen Bonds

In the previous sections we have described acid–base complexes in the solid state where dielectric constants are small, or in freon solvent mixtures around 130 K, where the dielectric constants are large.[30b] However, in the case of these mixtures, the dielectric constants decrease strongly when temperature is increased.

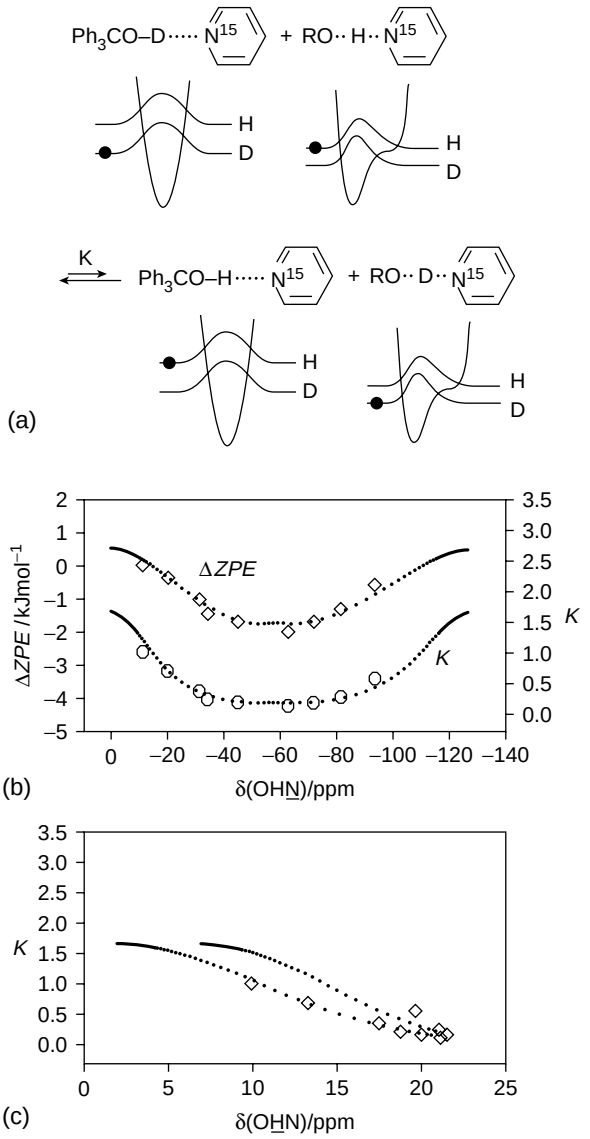

FIGURE 7.13 (a) Isotopic fractionation between acid–pyridine complexes and the reference triphenylmethanol–pyridine complex studied in Ref. 29 around 130 K using CDF_3/CDF_2Cl as solvent. (b) Values of *K* (circles) and zero-point energy differences ΔZPE (squares) as a function of the ^{15}N chemical shifts of hydrogen bonded pyridin–acid complexes. (c) Fractionation factors *K* as a function of the proton chemical shifts. The dotted lines were calculated as described in the text. (*Source*: From Limbach, H. H., Pietrzak, M., Sharif, S., Tolstoy, P. M., Shenderovich, I. G., Smirnov, S. N., Golubev, N. S., Denisov, G. S., NMR- parameters and geometries of OHN- and ODN hydrogen bonds of pyridine–acid complexes. *Chem. Eur. J.*, 10, 5195–5204, 2004. With permission.)

As a model system for this kind of problem Golubev et al.[21] have studied various hydrogen bonded complexes of HF with collidine–^{15}N in CDF_3/CDF_2Cl (Figure 7.14 top). The chemical shifts and coupling constants were obtained again by low-temperature NMR using CDF_3/CDF_2Cl as solvent, in particular by the influence of temperature, as these solvent mixtures exhibit a strong increase of the dielectric constant ε with decreasing temperature.[30b] The particular interest

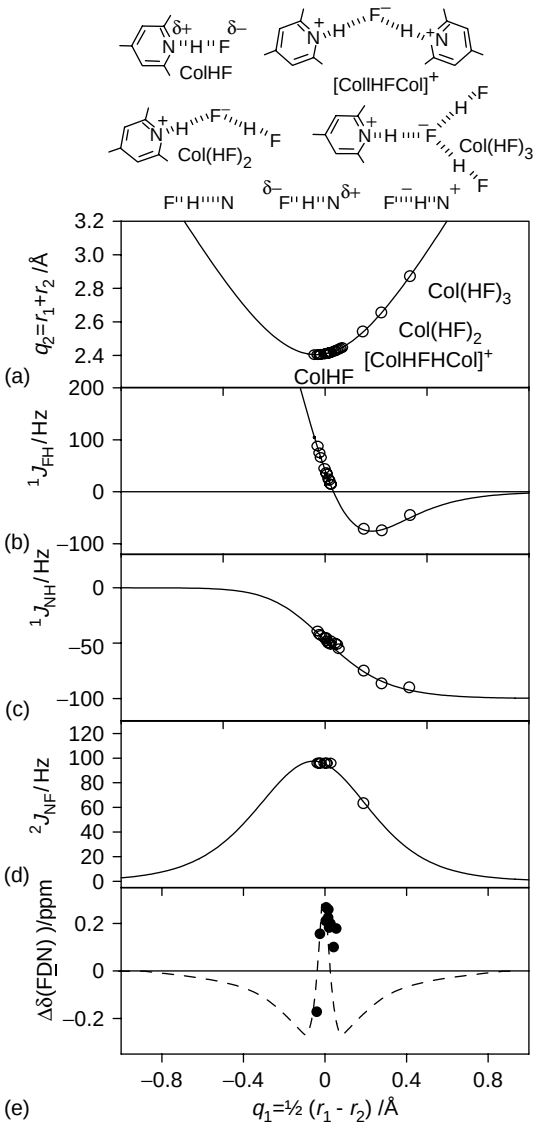

FIGURE 7.14 Hydrogen bond correlation $q_2 = f(q_1)$ for FHN systems. (a) Plot of the experimental coupling constants $^1J_{FH}$ (b), $^1J_{HN}$ (c) and $^2J_{FN}$ (d) and the primary isotope chemical shift effect $\Delta\delta$(FDN) (e) as a function of q_1. The solid lines are calculated according to the valence bond model as described in the text. (*Source*: From Shenderovich, I. G., Tolstoy, P. M., Golubev, N. S., Smirnov, S. N., Denisov, G. S., and Limbach, H. H., Low-temperature NMR studies of the structure and dynamics of a novel series of acid–base complexes of HF with collidine exhibiting scalar couplings across hydrogen bonds, *J. Am. Chem. Soc.*, 125, 11710–11720, 2003. With permission.)

in the FHN bond is that it resembles OHN bonds, but that ^{19}F exhibits a spin 1/2, so that by ^{15}N enrichment hydrogen bonds with three spins 1/2 can be realized. This allows one to measure coupling constants across hydrogen bonds in a similar way as for clusters of HF with F^-.[9]

The NMR parameters of the FHN hydrogen bonds obtained have been linked to the corresponding hydrogen bond geometries in Ref. 30a as depicted in Figure 7.14a which shows the geometric FHN hydrogen bond correlation as a function of q_1. Figure 7.14b to d refer to

the evolution of the experimental hydrogen bond coupling constants $^{1}J_{FH}$, $^{1}J_{HN}$ and $^{2}J_{FN}$. Furthermore, they are important NMR tools for the study of hydrogen bonds themselves, as well as for their theoretical description (see chapter of Del Bene).

Finally, the primary isotope chemical shift effect $\Delta\delta(F\underline{D}N) \equiv \delta(F\underline{D}N) - \delta(F\underline{H}N)$ on the hydron chemical shifts of the complex collidine–HF is depicted in Figure 7.14e, but will be discussed in the following.

In order to demonstrate the power of the method some typical multinuclear NMR signals of the collidine–HF and –DF complexes are depicted in Figure 7.15. The chemical shift of the bonding hydron (proton or deuteron) strongly depends on temperature and exhibits a maximum at the lowest reachable one, i.e., 103 K (Figure 7.15a and b). Primary isotope effects on the chemical shifts $\Delta\delta(F\underline{D}N) \equiv \delta(F\underline{D}N) - \delta(F\underline{H}N)$ are observed which are positive except at the highest temperature of 190 K where resolved signals could be obtained. A similar chemical shift dependence is observed for ^{19}F (Figure 7.15a and b). However, it is interesting to note that the secondary isotope effect on

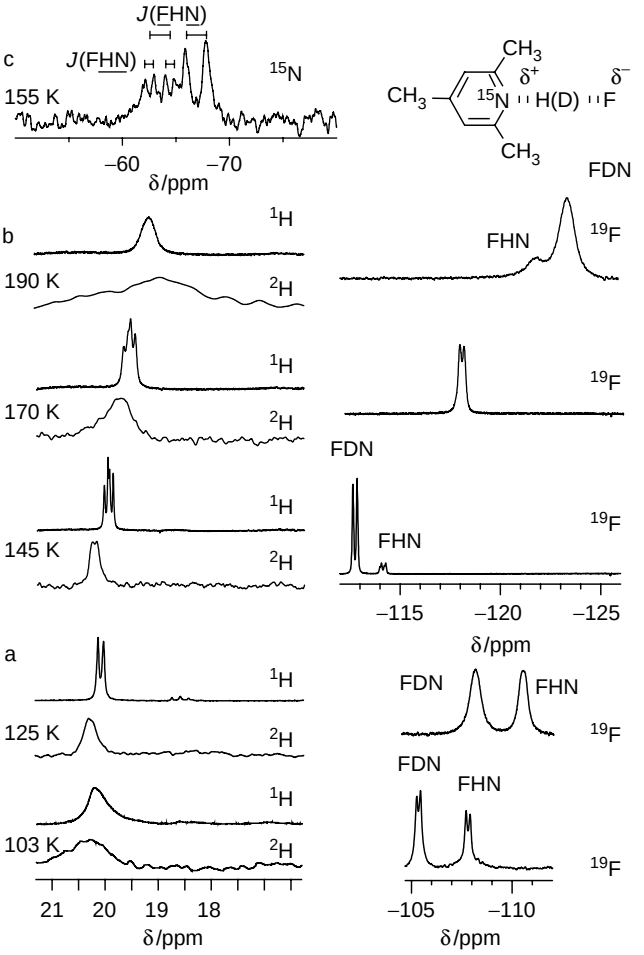

FIGURE 7.15 ^{1}H, ^{2}H, ^{15}N and ^{19}F NMR spectra of 1:1 complexes FHN and FDN between ^{15}N–collidine and HF/DF in $CDF_3/CDClF_2$. The deuterium fraction: 55% (a and c) and 85% (b). (*Source*: From Shenderovich, I. G., Burtsev, A. P., Denisov, G. S., Golubev, N. S., and Limbach, H. H., Influence of the temperature-dependent dielectric constant on the H/D isotope effects on the NMR chemical shifts and the hydrogen bond geometry of the collidine-HF complex in $CDF_3/CDClF_2$ solution, *Magn. Reson. Chem.*, 39, S91–S99, 2001. With permission.)

the ^{19}F chemical shift, $\Delta\delta(\underline{F}DN) \equiv \delta(\underline{F}DN) - \delta(\underline{F}HN)$, is positive at low temperatures, becomes immeasurably small at 170 K, and changes its sign at higher temperature. ^{15}N NMR spectra of FHN/FDN mixtures were obtained only around 155 K (Figure 7.15c). The secondary isotope effect for the nitrogen nucleus, $\Delta\delta(FD\underline{N}) \equiv \delta(FD\underline{N}) - \delta(FH\underline{N})$, is negative in this case. The NHF complex does not only exhibit large scalar couplings J_{FH} and J_{HN} but also a large value of J_{FN} around |96| Hz.[21] The changes in the one- and two-bond coupling constants across the FHN hydrogen bond observed experimentally for FH···collidine as a function of temperature have been supported by the results of an *ab initio* EOM–CCSD study of these coupling constants for FH–NH and FH–pyridine, which were used as models for FH–collidine.[45]

In Figure 7.16a we have plotted the secondary isotope effects on the fluorine chemical shifts $\Delta\delta(\underline{F}DN) \equiv \delta(\underline{F}DN) - \delta(\underline{F}HN)$ as a function of the dielectric constant which strongly increases with decreasing temperature. $\Delta\delta(\underline{F}DN)$ is negative at high temperatures, indicating that D is closer to F than H. However, at higher dielectric constants the effect becomes opposite, i.e., D is now farther away from F than H. We expect that if we could increase the solvent polarity to a very high

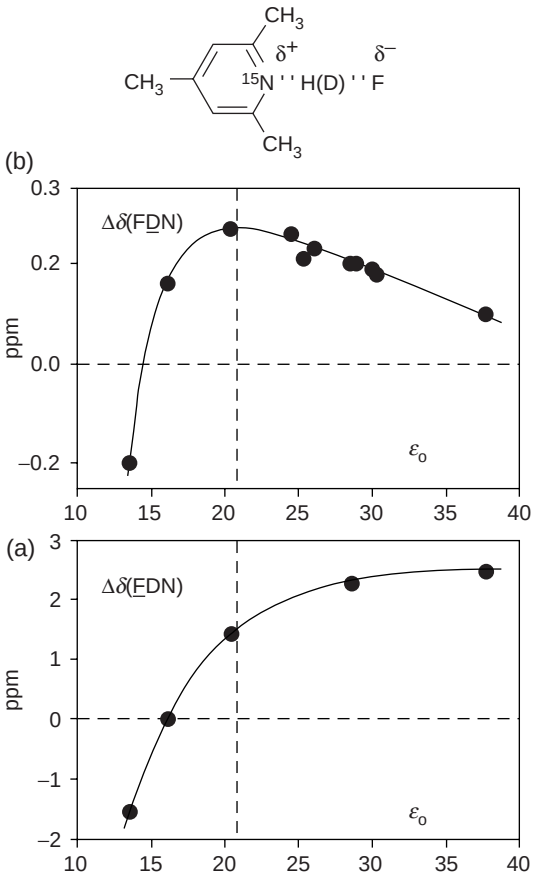

FIGURE 7.16 NMR parameters of the FHN and FDN complex dissolved in $CDF_3/CDClF_2$ mixtures as a function of the dielectric constant ε_o. (a) Secondary, $\Delta\delta(FD\underline{N}) \equiv \delta(FD\underline{N}) - \delta(FH\underline{N})$, H/D and (b) Primary, $\Delta\delta(FDN) \equiv \delta(FDN) - \delta(FHN)$, H/D isotope effects on the NMR chemical shifts. (*Source*: From Shenderovich, I. G., Burtsev, A. P., Denisov, G. S., Golubev, N. S., and Limbach, H. H., Influence of the temperature-dependent dielectric constant on the H/D isotope effects on the NMR chemical shifts and the hydrogen bond geometry of the collidine-HF complex in $CDF_3/CDClF_2$ solution, *Magn. Reson. Chem.*, 39, S91–S99, 2001. With permission.)

value $\Delta\delta(\underline{F}DN)$ would again become smaller. As far as the corresponding nitrogen value is concerned, we obtained only a single value of $\Delta\delta(FD\underline{N}) \equiv \delta(FD\underline{N}) - \delta(FH\underline{N}) = -3.36$ ppm at 155 K, indicating that D is closer to N than H.

In Figure 7.16b are depicted the primary isotope effects, $\Delta\delta(F\underline{D}N) \equiv \delta(F\underline{D}N) - \delta(F\underline{H}N)$ as a function of the dielectric constant of the solvent mixture, which is strongly dependent on temperature. The values are the same as in Figure 7.14e, where they had been plotted as a function of q_1. The values are found to be negative at high temperatures, i.e., low dielectric constants, indicating a situation where the deuteron is farther away from the hydrogen bond center than the proton. This finding is in agreement with the behavior of $\Delta\delta(\underline{F}DN)$, and expected for a situation prior to the formation of the quasisymmetric complex. When the dielectric constant is increased by lowering the temperature, $\Delta\delta(F\underline{D}N)$ crosses zero at $\varepsilon_o \approx 15$, goes through a maximum value of 0.27 ppm at ε_o around 22 and then decreases again. This value is comparable to the value of 0.32 ppm found for FHF^-.[41] We estimate that this maximum is the best characterization of a chemically asymmetric hydrogen bonded complex, where the single well potential for the proton, averaged over all various solvent environments is the most symmetric one, although H does not need to be located directly in the H-bond center as indicated in Figure 7.14e. These results support the situation depicted in Figure 7.2b, where the increase of the solvent polarity symmetrizes a hydrogen bond rather than to lower the symmetry.

D. H/D Isotope Effects on the NMR Parameters and Geometries of Coupled Hydrogen Bonds

Up to now, we have dealt only with hydrogen bonded systems containing single hydrogen bonds. In this section, we will deal with systems where several hydrogen bonds are coupled. Naturally, these systems are still far away from complex systems like water exhibiting an infinite number of coupled hydrogen bonds.

One can distinguish among the coupled hydrogen bonds cooperative and anticooperative bonds. In terms of hydrogen bond geometries this means that if the hydrogen coordinate *s*, defined in Figure 7.1a, of one hydrogen bond length is changed, the coordinate of a cooperatively coupled hydrogen bond is changed in the same and in an anticooperative coupled hydrogen bond in the opposite way as is illustrated in Figure 7.17. The two hydrogen bonds are uncoupled if a change of the geometry of one bond has no effect on the geometry of the other.

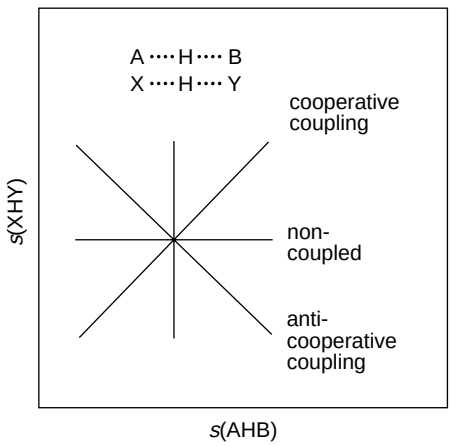

FIGURE 7.17 Cooperative and anticooperative coupling of two hydrogen bonds. For further explanation see text.

A convenient way to determine these effects is NMR spectroscopy combined with hydrogen bond correlations which are able to link NMR parameters with hydrogen bond geometries. As an example, we refer to a recent paper of Tolstoy et al.[43] of a low-temperature NMR study of acetic acid–acetate complexes in CDF_3/CDF_2Cl. Using appropriate chemical shift – geometry correlations similar to those discussed in the previous sections, the hydrogen bond geometries of the acetic acid dimer and of the acetate–acetic acid 1:2 complex (dihydrogen triacetate) were obtained. The distance changes after partial and full deuteration of the acetic acid dimer are depicted in Figure 7.18. Substitution of both H by D leads to a decrease of the shorter and an increase of the longer oxygen–hydrogen distances, where the overall average symmetry of the dimer is the same in the HH and the DD isotopologs. By contrast, the symmetry of the HD species is reduced as indicated in the geometry of the HD isotopolog depicted in Figure 7.18. Thus, the two hydrogen bonds in the cyclic dimer are cooperative.

In contrast to acetic acid cyclic dimer, the hydrogen bonds in dihydrogen triacetate are anticooperative. This is manifested in a low-field shift of a given hydrogen bond proton signal upon deuteration of the neighboring bonds. The corresponding geometric change of this OHO group is indicated in Figure 7.18. Now, the shorter OH distance is lengthened and the longer H···O distance shortened. Unfortunately, it was not possible to establish the geometric changes of the ODO group in a quantitative way, as the deuterium signal of the HD species could not be resolved.

In a similar way, the NMR parameters and the hydrogen bond geometries of the isotopologs of $[(FH)_nF]^-$ clusters in CDF_3/CDF_2Cl have been determined by low-temperature NMR[46] depicted schematically in Figure 7.19; $[FHF]^-$ and $[FDF]^-$ have been studied by Del Bene et al.[47] (see also chapter by Del Bene) as well as recently by Golubev et al. using quantum-mechanical methods.[28]

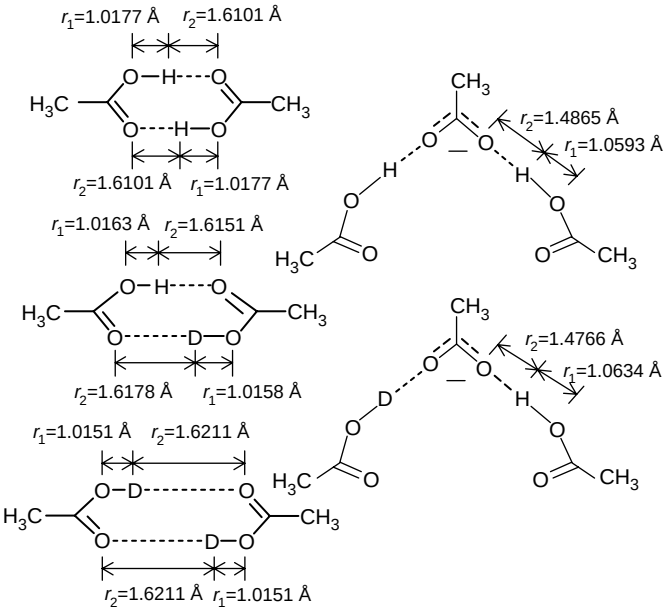

FIGURE 7.18 Hydrogen bond geometries of the three isotopologs of the cyclic dimer of acetic acid and of the two isotopologs of dihydrogen triacetate in CDF_3/CDF_2Cl obtained from ^1H and ^2H NMR chemicals shifts in Ref. 43. (*Source*: From Tolstoy, P. M., Schah-Mohammedi, P., Smirnov, S. N., Golubev, N. S., Denisov, G. S., and Limbach, H. H., Characterization of fluxional hydrogen bonded complexes of acetic acid and acetate by NMR: geometries, isotope and solvent effects, *J. Am. Chem. Soc.*, 126, 5621–5634, 2004. With permission.)

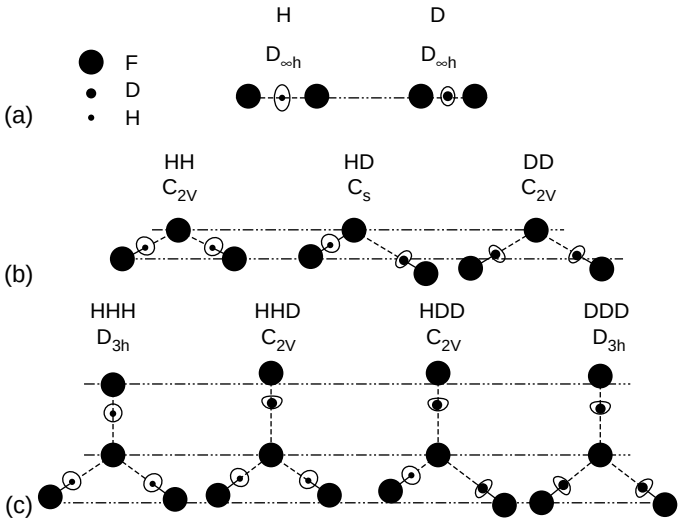

FIGURE 7.19 Hydrogen bond geometries of the isotopologs of $[(FH)_nF]^-$ clusters according to Ref. 46. (*Source*: From Shenderovich, I. G., Limbach, H. H., Smirnov, S. N., Tolstoy, P. M., Denisov, G. S., and Golubev, N. S., H/D isotope effects on the low-temperature NMR parameters and hydrogen bond geometries of $(FH)_2F^-$ and $(FH)_3F^-$ anions in CDF_3/CDF_2Cl liquid solution, *Phys. Chem. Chem. Phys.*, 4, 5488–5497, 2002. With permission.)

The F···F distance is by 0.0054 Å smaller for the latter,[48] which would already lead to a small low-field shift of D as compared to H. On the other hand, as illustrated in Figure 7.19a, D is more confined in the hydrogen bond center than H because of the smaller amplitudes of the vibrational ground-state stretching and bending vibrations, which contributes to the low-field shift of D as compared to H.

Calculations of isotope effects on the higher clusters are difficult and have not been performed up to date. Therefore, the NMR experiments give a first glance of what happens to the hydrogen bond geometries after deuteration. Especially useful are the coupling constants J_{FF} which were correlated with calculated equilibrium values of q_1 and q_2. Figure 7.19b depicts the case of $[FLFLF]^-$. Single deuteration of a given bond leads to an increase of the F···F distance of that bond, and a displacement of D towards the external F atom. The remaining FHF bond is, however, shortened indicating an anticooperative coupling. When this bond is also deuterated, the both F···F distances are the same and larger as compared to the nondeuterated isotopolog. The two deuterons are shifted somewhat back to the hydrogen bond center, as compared to D in the partially deuterated isotopolog. Similar effects, but less pronounced, are found for the $[(FH)_3F]^-$ cluster as depicted in Figure 7.19c.

These changes were quantified as illustrated Figure 7.20 in further detail. Here, the solid lines correspond to "direct" or primary H/D isotope effects and broken lines to "vicinal" effects. We note that the isotope effects on q_1 and on q_2 calculated from the observed H/D isotope effects on the coupling constants J_{FF} are similar for both clusters, which is not surprising in view of the correlation between both quantities which is linear in short intervals. The increase of the q_2 values after complete deuteration is 0.0022 Å for deuterated $(FD)_2F^-$ and 0.0035 Å for $(FD)_3F^-$. This change is opposite to the change in FLF^-. The corresponding increases of the distance q_1 of D to the H-bond center are 0.0032 Å and 0.0027 Å. Most interestingly are the partially deuterated complexes. Single H/D substitution in a given hydrogen bond leads to a substantial increase of the F···F distance and a substantial asymmetrization, i.e., increase of the distance of the deuteron from the H-bond center. On the other hand, we find also a significant decrease of the F···F distance

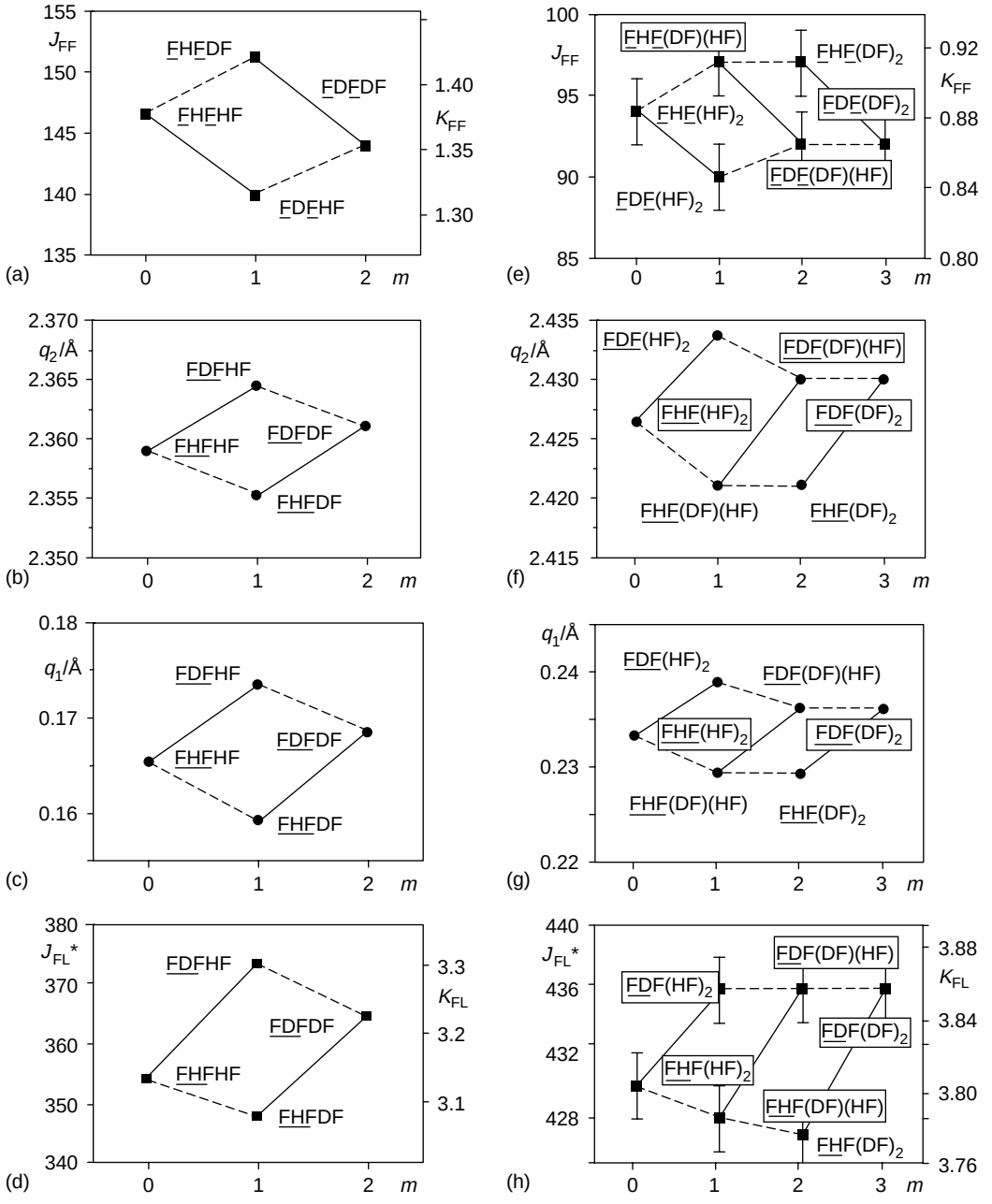

FIGURE 7.20 Coupling constants and hydrogen bond coordinates of $(FL)_2F^-$ and $(FL)_3F^-$ (L = H,D) as a function of the number m of deuterons in the complexes. (a, e): scalar coupling constants J_{FF}/Hz and reduced couplings $K_{FF}/10^{20}$ T^2J^{-1}. (b,c and f,g) hydrogen bond coordinates, (d,h) fluorine–hydron couplings $J^*_{FL} = J_{FL}\gamma_H/\gamma_L$ as well as the corresponding reduced couplings $K_{FL} = \gamma_H\gamma_L J_{FL}$ [10^{20} T^2J^{-1}]. Full lines depict the direct isotope effect, and the vicinal isotope effects are denoted by dotted lines. For further explanation see text. Reproduced with permission from Ref. 46.

and a decrease of the hydron distance from H-bond center when single H/D substitution occurs in a neighboring H-bond. These single H/D effects are larger than the overall double HH/DD isotope effects. In the case of $(FD)_3F^-$ it seems that substitution of the last H by D exhibits no isotope effect.

We come now to the, at first sight surprising, symmetry of the parallelograms in Figure 7.20 which indicate that for a given quantity, NMR parameter or hydrogen bond coordinate V, the following "sum rules" are valid:

$$V_H(HH) + V_D(DD) = V_H(HD) + V_D(DH) \tag{7.16}$$

$$V_H(HHH) + V_D(DDD) = V_H(HDD) + V_D(HHD) = V_H(HHD) + V_D(HDD) \tag{7.17}$$

where V_H refers to an FH···F bond and V_D to an FD···F bond. In other words, the resulting effect of total (double or triple) deuteration corresponds approximately to the algebraic sum of the direct (or one-bond) and the vicinal (or secondary) isotope effects. Or, for every parameter, the average value over all isotopologs belonging to a definite local point group is constant. We note that the sum rules found in this paper for NMR parameters and H-bond geometries coincide with the well-known sum rules for vibrational frequencies.[49] We also note that sum rules have been previously established for other systems, e.g., the chemical shifts of methane H/D isotopologs[50a] and of ammonia,[50b] but deviations were observed for ammonium.[50c]

The isotopic sum rules can facilitate considerably the assignment of spectral lines to given H/D isotopologs when scalar couplings across hydrogen bonds are absent, e.g., in the case of systems of hydrogen bonded complexes of the OHO type. The problem of line identification is especially important for isotopic modifications of hydrogen bonded systems, which cannot be studied separately but only as an equilibrium mixture. In addition, the rule provides grounds of the method of determination proposed in Ref. 51 of the composition of hydrogen bonded associates using the multiplicity of isotopic splitting. In particular, it excludes the possibility of occasional coincidence of several lines in such an isotopic multiplet.

As the sum rules are valid for so many different quantities, they arise most probably, from a similar origin. On the other hand, the sum rules as well as the analogous product rules for vibrational frequencies were derived in harmonic approximation, whereas the isotope effects on the NMR parameters and on H-bond geometries are essentially caused by anharmonic effect. A consideration of this problem in terms of perturbation theory will be given elsewhere.

These results of this section may be only semiquantitative and subject to systematic errors, but may motivate a theoretical chemist to study these ions in a quantitative way in the future, which justifies the use of the simple chemical shift – geometry correlations.

IV. CONCLUSIONS

We conclude that liquid- and solid-state NMR spectroscopy constitutes a very important tool for the study of isotope effects of strong hydrogen bonds. The latter do not only play an important role with respect to the function of hydrogen bonds but also represent models for the transition states of high-barrier proton-transfer reactions. By introducing appropriate correction terms into the bond valence analysis a proper description of geometric hydrogen bond correlations both for protonated as well as for deuterated systems is achieved. By dipolar NMR the world of hydrogen bond geometries and NMR parameters are linked together. By low-temperature liquid-state NMR intrinsic NMR parameters of systems with single or coupled hydrogen bonds can be studied in the slow hydrogen bond exchange regime. This combination allows one to convert isotope effects on NMR parameters — which can be measured with a high precision — into isotope effects on hydrogen bond geometries.

ACKNOWLEDGMENTS

This research has been supported by the Deutsche Forschungsgemeinschaft, Bonn, the Fonds der Chemischen Industrie (Frankfurt) and the Russian Foundation of Basic Research, grant 03-03-04009. We are indebted to Prof. Janet Del Bene, Youngstown State University, and Prof. Charles Perrin, University of California, San Diego, for helpful comments and proofreading of this manuscript.

REFERENCES

1 Denisov, G. S., Bureiko, S. F., Golubev, N. S., and Tokhadze, K. G., The kinetics of exchange and proton transfer processes in hydrogen-bonded systems in inert media, In *Molecular Interactions*, Vol. 2, Ratajczak, H. and Orville-Thomas, W. J., Eds., Wiley, New York, pp. 107–141, 1981.

2 (a) Limbach, H. H., *Dynamic NMR Spectroscopy in the Presence of Kinetic Hydrogen/Deuterium Isotope Effects*, *NMR Basic Principles and Progress, Deuterium and Shift Calculation*, Vol. 23, Springer-Verlag, Heidelberg, pp. 66–167, 1991; (b) Limbach, H. H., Dynamics of hydrogen transfer in liquids and solids, In *Encyclopedia of Nuclear Magnetic Resonance*, *Advances in NMR*, Suppl. Vol. 9, Grant, D. M. and Harris, R. K., Eds., Wiley, Chichester, pp. 520–531, 2002.

3 Denisov, G. S. and Golubev, N. S., Localization and moving of proton inside hydrogen bonded complexes in aprotic solvents, *J. Mol. Struct.*, 75, 311–326, 1981.

4 Steiner, T., *Angew. Chem. Int. Ed.*, 41, 48–76, 2002.

5 (a) Pauling, L., Atomic radii and interatomic distances in metals, *J. Am. Chem. Soc.*, 69, 542–553, 1947; (b) Brown, I. D., Chemical and steric constraints in inorganic solids, *Acta Cryst.*, B48, 553–572, 1992.

6 (a) Truhlar, D. G., Test of bond-order methods for predicting position of minimum-energy path for hydrogen atom transfer reactions, *J. Am. Chem. Soc.*, 94, 7584–7586, 1972, (b) Agmon, N., Generating reaction coordinates by Pauling relation, *Chem. Phys. Lett.*, 45, 343–345, 1977.

7 (a) Steiner, T. and Saenger, W., Covalent bond lengthening in hydroxyl groups involved in three-center and in cooperative hydrogen bonds. Analysis of low-temperature neutron diffraction data, *J. Am. Chem. Soc.*, 114, 7123–7126, 1992, (b) Steiner, T. and Saenger, W., Lengthening of the covalent O–H Bond in O–H···O hydrogen bonds reexamined from low-temperature neutron diffraction data of organic compounds, *Acta Cryst.*, B50, 348–357, 1994, (c) Steiner, T., Lengthening of the N–H bond in NHN hydrogen bonds. Preliminary structural data and implications of the bond valence concept, *J. Chem. Soc., Chem. Commun.*, 1331–1332, 1995, (d) Steiner, T., Lengthening of the covalent X–H bond in heteronuclear hydrogen bonds quantified from organic and organometallic neutron crystal structures, *J. Phys. Chem. A*, 102, 7041–7052, 1998.

8 Benedict, H., Limbach, H. H., Wehlan, M., Fehlhammer, W. P., Golubev, N. S., and Janoschek, R., Solid state ^{15}N NMR and theoretical studies of *primary* and *secondary* geometric H/D isotope effects on low-barrier NHN-hydrogen bonds, *J. Am. Chem. Soc.*, 120, 2939–2950, 1998.

9 Shenderovich, I. G., Smirnov, S. N., Denisov, G. S., Gindin, V. A., Golubev, N. S., Dunger, A., Reibke, R., Kirpekar, S., Malkina, O. L., and Limbach, H. H., Nuclear magnetic resonance of hydrogen bonded clusters between F^- and $(HF)_n$: experiment and theory, *Ber. Bunsenges. Phys. Chem.*, 102, 422–428, 1998.

10 (a) Ramos, M., Alkorta, I., Elguero, J., Golubev, N. S., Denisov, G. S., Benedict, H., and Limbach, H. H., Theoretical study of the influence of electric fields on hydrogen-bonded acid–base complexes, *J. Phys. Chem. A*, 101, 9791–9800, 1997, (b) Picazo, O., Alkorta, I., and Elguero, J., Large chiral recognition in hydrogen-bonded complexes and proton transfer in pyrrolo[2,3-*b*]pyrrole dimers as model compounds, *J. Org. Chem.*, 68, 7485–7489, 2003.

11 (a) Sokolov, N. D., Vener, M. V., and Savel'ev, V. A., Tentative study of strong hydrogen bond dynamics. Vibrational frequency considerations, *J. Mol. Struct.*, 222, 365–386, 1990, and references cited therein, (b) Basilevsky, M. V. and Vener, M. V., Theoretical investigations of proton and hydrogen atom transfer in the condensed phase, *Russ. Chem. Rev.*, 72, 1–33, 2003.

12 (a) Redington, R. L. and Sams, R. L., State-specific spectral doublets in the FTIR spectrum of gaseous tropolone, *J. Phys. Chem. B*, 106, 7494–7511, 2002, (b) Rowe, W. F., Duerst, R. W., and Wilson, E. B.,

The intramolecular hydrogen bond in malonaldehyde, *J. Am. Chem. Soc.*, 98, 4021–4023, 1976, (c) Meyer, R. and Ha, T. K., Quantum states of hydrogen transfer and vibration in malonaldehyde, *Mol. Phys.*, 101, 3263–3276, 2003.

13 (a) Firth, D. W., Barbara, P. F., and Trommsdorff, H. P., Matrix induced localization of proton tunneling in malonaldehyde, *Chem. Phys.*, 136, 349–360, 1989, (b) Wehrle, B., Zimmermann, H., and Limbach, H. H., A solid state ^{15}N CPMAS NMR study of dye tautomerism in glassy polystyrene: site dependence of double minimum potentials and their motional averaging, *J. Am. Chem. Soc.*, 110, 7014–7024, 1988.

14 Madeja, F. and Havenith, M., High resolution spectroscopy of carboxylic acid in the gas phase: observation of proton transfer in $(DCOOH)_2$, *J. Chem. Phys.*, 117, 7162–7168, 2004.

15 Xue, Q., Horsewill, A. J., Johnson, M. R., and Trommsdorff, H. P., Isotope effects associated with tunneling and double proton transfer in the hydrogen bonds of benzoic acid, *J. Chem. Phys.*, 120, 11107–11118, 2004.

16 (a) Perrin, C. L. and Thoburn, J. D., Symmetries of hydrogen bonds in monoanions of dicarboxylic acids, *J. Am. Chem. Soc.*, 114, 8559–8565, 1992, (b) Perrin, C. L., Symmetries of hydrogen bonds in solution, *Science*, 266, 1665–1668, 1994, (c) Perrin, C. L., Nielson, J. B., and Kim, Y. J., Symmetry of hydrogen bonds in solution, an overview, *Ber. Bunsenges. Phys. Chem.*, 102, 403–409, 1998, (d) Perrin, C. L. and Kim, Y. J., Symmetry of the hydrogen bond in malonaldehyde enol in solution, *J. Am. Chem. Soc.*, 120, 12641–12645, 1998, (e) Perrin, C. L., and Nielson, J. B., Asymmetry of hydrogen bonds in solutions of monoanions of dicarboxylic acids, *J. Am. Chem. Soc.*, 119, 12734–12741, 1997, (f) Perrin, C. L. and Nielson, J. B., Strong hydrogen bonds in chemistry and biology, *Annu. Rev. Phys. Chem.*, 48, 511–544, 1997.

17 (a) Rumpel, H. and Limbach, H. H., NMR study of kinetic HH/HD/DD isotope, solvent, and solid-state effects on double proton transfer in azophenine, *J. Am. Chem. Soc.*, 111, 5429–5441, 1989, (b) Rumpel, H., Limbach, H. H., and Zachmann, G., Liquid- and solid-state IR and NIR study of the proton dynamics in azophenine, *J. Phys. Chem.*, 93, 1812–1818, 1989.

18 Geppert, S., Rabold, A., Zundel, G., and Eckert, M., Theoretical treatment of spectroscopic data for a strong hydrogen bond with a broad single-minimum proton potential, *J. Phys. Chem.*, 99, 12220–12224, 1995, and references cited therein.

19 (a) Smirnov, S. N., Golubev, N. S., Denisov, G. S., Benedict, H., Schah-Mohammedi, P., and Limbach, H. H., Hydrogen/deuterium isotope effects on the NMR chemical shifts and geometries of intermolecular low-barrier hydrogen bonded complexes, *J. Am. Chem. Soc.*, 118, 4094–4101, 1996, (b) Golubev, N. S., Smirnov, S. N., Gindin, V. A., Denisov, G. S., Benedict, H., and Limbach, H. H., Formation of charge relay chains between acetic acid and pyridine observed by low-temperature NMR, *J. Am. Chem. Soc.*, 116, 12055–12056, 1994, (c) Golubev, N. S., Denisov, G. S., Smirnov, S. N., Shchepkin, D. N., and Limbach, H. H., Evidence by NMR of temperature-dependent solvent electric field effects on proton transfer and hydrogen bond geometries, *Z. Phys. Chem.*, 196, 73–84, 1996.

20 (a) Del Bene, J. E., Jordan, M. J. T., Gill, P. M. W., and Buckingham, A. D., An ab initio study of anharmonicity and matrix effects on the hydrogen-bonded $BrH{:}NH_3$ complex, *Mol. Phys.*, 92, 429–439, 1997, (b) Jordan, M. J. T. and Del Bene, J. E., Unraveling environmental effects on hydrogen-bonded complexes: matrix effects on the structures and proton-stretching frequencies of hydrogen-halide complexes with ammonia and trimethylamine, *J. Am. Chem. Soc.*, 122, 2101–2115, 2000, (c) Del Bene, J. E. and Jordan, M. J. T., Vibrational spectroscopy of the hydrogen bond: an ab initio quantum-chemical perspective, *Int. Rev. Phys. Chem.*, 18, 119–162, 1999.

21 Golubev, N. S., Shenderovich, I. G., Smirnov, S. N., Denisov, G. S., and Limbach, H. H., Nuclear scalar spin–spin coupling reveals novel properties of low-barrier hydrogen bonds in a polar environment, *Chem. Eur. J.*, 5, 492–497, 1999.

22 Limbach, H. H., Pietrzak, M., Benedict, H., Tolstoy, P. M., Golubev, N. S., and Denisov, G. S., Empirical corrections for anharmonic zero-point vibrations of hydrogen and deuterium in geometric hydrogen bond correlations, *J. Mol. Struct.*, 706, 115–119, 2004.

23 (a) Ubbelohde, A. R. and Gallagher, K. G., Acid–base effects in hydrogen bonds in crystals, *Acta Cryst.*, 8, 71–83, 1955, (b) Legon, A. C. and Millen, D. J., Systematic effect of D substitution on hydrogen-bond lengths in gas-phase dimers B···HX and a model for its interpretation, *Chem. Phys. Lett.*, 147, 484–489, 1988, (c) Sokolov, N. D. and Savel'ev, V. A., Dynamics of hydrogen bond: two-dimensional model and isotope effects, *Chem. Phys.*, 22, 383–399, 1977, (d) Sokolov, N. D. and

Savel'ev, V. A., Isotope effects in weak hydrogen bonds. Allowance for two stretching and two bending modes of the A–H···B fragment, *Chem. Phys.*, 181, 305–317, 1994.
24 Lutz, H. D., Hydroxide ions in condensed materials — correlation of spectroscopic and structural data, *Struct. Bond. (Berlin)*, 82, 85–103, 1995.
25 Lutz, H. D., Structure and strength of hydrogen bonds in inorganic solids, *J. Mol. Struct.*, 646, 227–236, 2003.
26 Lutz, H. D. and Engelen, B., Hydrogen Bonds in Inorganic Solids, *Trends in Applied Spectroscopy*, 4, 355–375, 2002.
27 (a) Almlöf, J., Hydrogen bond studies. Ab-initio calculation of vibrational structure and equilibrium geometry in HF_2^- and DF_2^-, *Chem. Phys. Lett.*, 17, 49–52, 1972, (b) Kawaguchi, K. and Hirota, E., Diode-laser spectroscopy of the ν_3 and ν_2 bands of FHF^- in 1300 cm^{-1} region, *J. Chem. Phys.*, 87, 6838–6841, 1987, (c) Kawaguchi, K. and Hirota, E., Infrared diode laser spectroscopy of FDF^-, *J. Mol. Struct.*, 352/353, 389–394, 1995.
28 Golubev, N. S., Melikova, S. M., Shchepkin, D. N., Shenderovich, I. G., Tolstoy, P. M., and Denisov, G. S., Interpretation of hydrogen/deuterium isotope effects on NMR chemical shifts of $[FHF]^-$ ion based on calculations of nuclear magnetic shielding tensor surface, *Z. Phys. Chem.*, 217, 1549–1563, 2003.
29 Smirnov, S. N., Benedict, H., Golubev, N. S., Denisov, G. S., Kreevoy, M. M., Schowen, R. L., and Limbach, H. H., Exploring zero-point energies and hydrogen bond geometries along proton transfer pathways by low-temperature NMR, *Can. J. Chem.*, 77, 943–949, 1999.
30 (a) Shenderovich, I. G., Tolstoy, P. M., Golubev, N. S., Smirnov, S. N., Denisov, G. S., and Limbach, H. H., Low-temperature NMR studies of the structure and dynamics of a novel series of acid–base complexes of HF with collidine exhibiting scalar couplings across hydrogen bonds, *J. Am. Chem. Soc.*, 125, 11710–11720, 2003, (b) Shenderovich, I. G., Burtsev, A. P., Denisov, G. S., Golubev, N. S., and Limbach, H. H., Influence of the temperature-dependent dielectric constant on the H/D isotope effects on the NMR chemical shifts and the hydrogen bond geometry of the collidine-HF complex in CDF_3/$CDClF_2$ solution, *Magn. Reson. Chem.*, 39, S91–S99, 2001.
31 (a) Kreevoy, M. M. and Liang, T. M., Structures and isotopic fractionation factors of complexes $A_1HA_2^-$, *J. Am. Chem. Soc.*, 102, 3315–3322, 1980, (b) Bone, R. and Wolfenden, R., Solvent isotope effects on formation of protease complexes with inhibitory aldehydes, *J. Am. Chem. Soc.*, 107, 4772–4777, 1985.
32 Harris, T. K., Abeygunawardana, C., and Mildvan, A. S., NMR studies of the role of hydrogen bonding in the mechanism of triosephosphate isomerase, *Biochemistry*, 36, 14661–14675, 1997.
33 (a) Somorjai, R. L. and Hornig, D. F., Double-minimum potentials in hydrogen-bonded solids, *J. Chem. Phys.*, 36, 1980–1987, 1962, (b) Janoschek, R., Weidemann, E. G., Pfeiffer, H., and Zundel, G., Extremely high polarizability of hydrogen bonds, *J. Am. Chem. Soc.*, 94, 2387–2396, 1972.
34 (a) Allen, F. H., Davies, J. E., Galloy, J. J., Johnson, O., Kennard, O., Macrae, C. F., Mitchell, E. M., Mitchell, G. F., Smith, J. M., and Watson, D. G., The development of version-3 and version-4 of the cambridge structural database system, *J. Chem. Inf. Comp. Sci.*, 31, 187–204, 1991, (b) Allen, F. H., The cambridge structural database: a quarter of a million crystal structures and rising, *Acta Cryst.*, B58, 380–388, 2002.
35 (a) Lorente, P., Shenderovich, I. G., Golubev, N. S., Denisov, G. S., Buntkowsky, G., and Limbach, H. H., $^1H/^{15}N$ NMR chemical shielding, dipolar ^{15}N, ^2H coupling and hydrogen bond geometry correlations in a novel series of hydrogen-bonded acid–base complexes of collidine with carboxylic acids, *Magn. Reson. Chem.*, 39, S18–S29, 2001, (b) Foces-Foces, C., Llamas-Saiz, A. L., Lorente, P., Golubev, N. S., and Limbach, H. H., Three 2,4,6-trimethylpyridine-benzoic acid complexes at 150 K, *Acta Cryst.*, C55, 377–381, 1999.
36 Tolstoy, P. M., Smirnov, S. N., Shenderovich, I. G., Golubev, N. S., Denisov, G. S., and Limbach, H. H., NMR studies of solid state-solvent and H/D isotope effects on hydrogen bond geometries of 1:1 complexes of collidine with carboxylic acids, *J. Mol. Struct.*, 700, 19–27, 2004.
37 Limbach, H. H., Pietrzak, M., Sharif, S., Tolstoy, P. M., Shenderovich, I. G., Smirnov, S. N., Golubev, N. S., Denisov, G. S., NMR parameters and geometries of OHN and ODN hydrogen bonds of pyridine–acid complexes. *Chem. Eur. J.*, 10, 5195–5204, 2004.
38 (a) Steiner, T., Majerz, I., and Wilson, C. C., First OHN hydrogen bond with a centered proton obtained by thermally induced proton migration, *Angew. Chem. Int. Ed.*, 40, 2651–2654, 2001, (b) Steiner, T.,

Wilson, C. C., and Majerz, I., Neutron diffraction study of a very short OHN hydrogen bond: crystalline adduct of 2-methylpyridine and pentachlorophenol, *Chem Commun*, 1231–1232, 2000.

39 Solid NH_4Cl has been shown to resonate at −341.168 ppm with respect to external liquid nitromethane by Hayashi, S. and Hayamizu, K., Chemical shift standards in high-resolution solid-state NMR. ^{15}N nuclei, *Bull. Chem. Soc. Jpn*, 64, 688–690, 1991.

40 Shenderovich, I. G., Buntkowsky, G., Schreiber, A., Gedat, E., Sharif, S., Albrecht, J., Golubev, N. S., Findenegg, G. H., and Limbach, H. H., Pyridine-^{15}N — a mobile NMR sensor for surface acidity and surface defects of mesoporous silica, *J. Phys. Chem. B*, 107, 11924–11939, 2003.

41 Schah-Mohammedi, P., Shenderovich, I. G., Detering, C., Limbach, H. H., Tolstoy, P. M., Smirnov, S. N., Denisov, G. S., and Golubev, N. S., Hydrogen/deuterium-isotope effects on NMR chemical shifts and symmetry of homoconjugated hydrogen-bonded ions in polar solution, *J. Am. Chem. Soc.*, 122, 12878–12879, 2000.

42 Emmler, T., Gieschler, S., Limbach, H. H., and Buntkowsky, G., A simple method for the characterization of OHO-hydrogen-bonds by ^{1}H-solid-state NMR spectroscopy, *J. Mol. Struct.*, 700, 29–38, 2004.

43 Tolstoy, P. M., Schah-Mohammedi, P., Smirnov, S. N., Golubev, N. S., Denisov, G. S., and Limbach, H. H., Characterization of fluxional hydrogen bonded complexes of acetic acid and acetate by NMR: geometries, isotope and solvent effects, *J. Am. Chem. Soc.*, 126, 5621–5634, 2004.

44 Melander, L. and Saunders, W. H., *Reaction rates of isotopic molecules*, Wiley, New York, Toronto, 1980.

45 Del Bene, J. E., Bartlett, R. J., and Elguero, J., Interpreting $^{2h}J(F,N)$, $^{1h}J(H,N)$ and $^{1}J(F,H)$ in the hydrogen-bonded FH:collidine complex, *Magn. Reson. Chem.*, 40, 767–771, 2002.

46 Shenderovich, I. G., Limbach, H. H., Smirnov, S. N., Tolstoy, P. M., Denisov, G. S., and Golubev, N. S., H/D isotope effects on the low-temperature NMR parameters and hydrogen bond geometries of $(FH)_2F^-$ and $(FH)_3F^-$anions in CDF_3/CDF_2Cl liquid solution, *Phys. Chem. Chem. Phys.*, 4, 5488–5497, 2002.

47 Del Bene, J. E., Jordan, M. J. T., Perera, S. A., and Bartlett, R. J., Vibrational effects on the F–F spin–spin coupling constant ($^{2h}J_{F-F}$) in FHF^- and FDF^-, *J. Phys. Chem. A*, 105, 8399–8402, 2001.

48 Kawaguchi, K. and Hirota, E., Infrared diode laser study of the hydrogen bifluoride anion: FHF^- and FDF^-, *J. Chem. Phys.*, 84, 2953–2960, 1986.

49 Wilson, E. B., Decius, J. C., and Cross, P. C., *Molecular Vibrations*, McGrow-Hill, London, 1955.

50 (a) Lazzeretti, P., Zanasi, R., Sadlej, A. J., and Raynes, W. T., Magnetizability and C-13 shielding surfaces for the methane molecule, *Mol. Phys.*, 62, 605–616, 1987, (b) Litchman, W. M., Alei, M., and Florin, A. E. ^{15}N NMR chemical shifts in $^{15}ND_3$, $^{15}ND_2H$, $^{15}NDH_2$, and $^{15}NH_3$, *J. Chem. Phys.*, 50, 1897–1898, 1969, (c) Hansen, P. E. and Lycka, A., A reinvestigation of one-bond deuterium isotope effects on nitrogen and on proton nuclear shielding for the ammonium ion, *Acta Chem. Scand.*, 43, 222–232, 1989.

51 Detering, C., Tolstoy, P. M., Golubev, N. S., Denisov, G. S., and Limbach, H. H. Vicinal H/D Isotope effects in NMR spectra of complexes with coupled hydrogen bonds. Phosphoric acids, *Dokl. Phys. Chem.*, 379, 191–193, 2001.